THERMAL MODELING OF A LOADED MAGNASTOR STORAGE SYSTEM AT CATAWBA NUCLEAR STATION

Fuel Cycle Research & Development

Prepared for
U.S. Department of Energy
Used Fuel Disposition Campaign

JA Fort
TE Michener
SR Suffield
DJ Richmond
September 29, 2016
FCRD-UFD-2016-000068
PNNL-25871 Rev. 0

Reviewed by:

PNNL Project Manager

Signature on file

_____

Brady Hanson

SUMMARY

This report represents fulfillment of the M2 Milestone M2FT-16PN080203031, "High Heat Load Thermal Analyses," under Work Package FT-16PN08020303. The report documents the analysis of the NAC International, Inc. (NAC) Modular, Advanced Generation, Nuclear All-purpose STORage (MAGNASTOR) module at Duke's Catawba Nuclear Station.

As part of the Used Fuel Disposition Campaign of the U.S. Department of Energy, a high-burnup fuel storage demonstration is planned for a storage module in the North Anna Nuclear Station's Independent Spent Fuel Storage Installation (ISFSI). The storage module selected for this demonstration is an AREVA TN-32B High Burnup cask. The main goals of this proposed test are to provide confirmatory data for model validation and potential improvement, support license renewals and new licenses for ISFSIs, and support transportation licensing for high burnup spent nuclear fuel (EPRI 2014). The focus of the Demonstration test is the performance of the high-burnup fuel. To support the High Burnup Spent Fuel Data Project, Pacific Northwest National Laboratory (PNNL) staff performed a detailed thermal analysis (Fort et al. 2016) of the TN-32B cask. It was found that when conservatisms were removed from the thermal models and especially from the calculated decay heats, the predicted peak cladding temperatures (PCTs) were significantly below the 400°C (752°F) regulatory guidance limit, as specified in Interim Staff Guidance 11, Revision 3, (U.S. NRC 2003).

The objective of the present study is to complete a thermal analysis of an additional storage system design with a typical loading of high burnup fuel. The predicted fuel cladding temperatures will be used for comparison with those estimated for the High Burnup Demonstration cask and will add to the knowledge of expected fuel temperatures in used fuel storage systems. The storage system selected for this study is a NAC MAGNASTOR located at the Catawba Nuclear Station ISFSI. The MAGNASTOR modeled is a dual purpose canister-based system with a basket designed to hold 37 pressurized water reactor (PWR) fuel assemblies. It consists of a transportable storage canister (TSC) with a welded closure, a ventilated concrete storage cask, and a transfer cask.

This report describes the models developed and results of thermal analyses using best estimate data provided by the utility, Duke Energy, fuel assembly design information provided by the fuel vendors, Westinghouse Electric Company and AREVA, and decay heat estimates for each rod from Oak Ridge National Laboratory (ORNL) based on actual power history data.

Detailed models of the MAGNASTOR storage module were developed using two codes, COBRA-SFS (Michener et al. 2015) and STAR-CCM+ (CD-adapco 2015). Estimates of fuel cladding temperatures were of primary interest, but temperatures of the storage system components were captured as well. While the two codes each model the entire storage system, each code is used to model different areas in detail. COBRA-SFS is used to model the fuel and basket region in detail, treating the external components in a more coarse fashion, whereas STAR-CCM+ is used to model the basket and surrounding components in detail, while treating the fuel in an averaged manner. Inputs for the treatment of the fuel region in the STAR-CCM+ model are provided through separate runs with COBRA-SFS and with model runs for an individual assembly in STAR-CCM+. With consistent material specifications and the same

ambient boundary conditions, these two models are complementary and consistency in results provides confidence in their accuracy.

Since this is an already-loaded storage module, the two independent models were set up with the objective of giving the most accurate representation of that specific canister in a MAGNASTOR storage system. Except for assumptions regarding ambient boundary conditions, the models produced for this study can be considered "best estimate". They omit many of the conservatisms and bounding assumptions normally used in design-basis and safety-basis calculations for spent fuel storage systems. Simulations for both models (COBRA-SFS and STAR-CCM+) were run for the initial loading and installation in August of 2014. Ambient conditions are the same used in the Final Safety Analysis Report (FSAR) (NAC 2011), which consisted of a 24°C (76°F) ambient with regulatory solar insolation. This temperature is representative of the mean ambient temperature at the Catawba site during August of 2014.

Additional simulations were run with COBRA-SFS to estimate fuel cladding temperatures at future dates, including 10, 50, 100, 200, and 300 years from the initial loading. These calculations used the same input data with the best estimate assembly decay heats for those dates. Appendix A provides a comparison of fuel cladding temperatures for a design basis heat loading and at initial loading using the conservative canister loading decay heat estimates provided by Duke Energy.

The distribution of peak assembly cladding temperatures calculated with the COBRA-SFS and STAR-CCM+ models for the initial loading, using best estimate decay heats, is shown in Figure S-1. Estimates produced with the two models are consistent. Generally higher predicted PCTs with STAR-CCM+ in the center assemblies may be credited to the more conservative nature of the effective thermal conductivity model used to represent the fuel assemblies. That conservatism also applies to the outer assemblies; however peak cladding temperatures in those assemblies are generally lower than predicted with COBRA-SFS. This was also observed in the TN-32B model results (Fort et al. 2016) and was attributed to the higher convective heat transfer predicted by STAR-CCM+ to the outer channels.

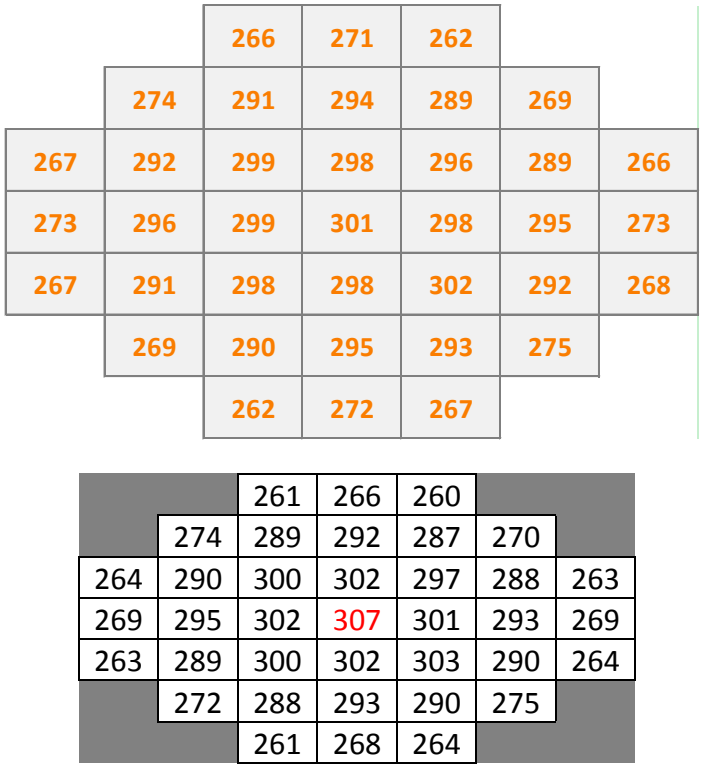

		266	271	262		
	274	291	294	289	269	
267	292	299	298	296	289	266
273	296	299	301	298	295	273
267	291	298	298	302	292	268
	269	290	295	293	275	
		262	272	267		

COBRA-SFS

		261	266	260		
	274	289	292	287	270	
264	290	300	302	297	288	263
269	295	302	307	301	293	269
263	289	300	302	303	290	264
	272	288	293	290	275	
		261	268	264		

STAR-CCM+

Figure S-1. Comparison of Peak Cladding Temperatures (°C) for both Models for the Initial Loading (August 2014) and Best Estimate Decay Heats

ACKNOWLEGMENTS

PNNL wishes to thank Duke Energy, NAC International, Inc., Westinghouse Electric Company, and AREVA Fuels for their cooperation and sharing of data information needed to complete thermal analyses. We also thank Henrik Liljenfeldt (ORNL) for ORIGEN calculations of decay heat and helpful explanations regarding assembly design. Finally we wish to acknowledge the careful attention that Colleen Winters and Susan Tackett provided to get the report into its final form.

ACRONYMS AND ABBREVIATIONS

ACWS	annulus cooling water system
BWR	boiling water reactor
CAD	computer aided design
CFD	computational fluid dynamics
DOE	U.S. Department of Energy
EPRI	Electric Power Research Institute
FSAR	final safety analysis report
GWd/MTU	gigawatt days per metric ton uranium (measure of burnup)
ISFSI	independent spent fuel storage installation
MAGNASTOR	Modular, Advanced Generation, Nuclear All-purpose STORage
NAC	NAC International, Inc.
NDA	non-disclosure agreement
ORNL	Oak Ridge National Laboratory
PCT	peak cladding temperature
PNNL	Pacific Northwest National Laboratory
PWR	pressurized water reactor
TSC	transportable storage canister
WE	Westinghouse Electric Company

CONTENTS

FIGURES

TABLES

THERMAL MODELING OF A LOADED MAGNASTOR STORAGE SYSTEM AT CATAWBA NUCLEAR STATION

1.0 INTRODUCTION

As part of the Used Fuel Disposition Campaign of the U.S. Department of Energy (DOE) and specifically for comparison with fuel temperatures predicted in the High Burnup Demonstration cask (Fort et al. 2016), thermal analyses have been completed for a storage module in the Catawba Nuclear Station's independent spent fuel storage installation (ISFSI). The storage module selected for this comparison is a NAC International, Inc. (NAC) Modular, Advanced Generation, Nuclear All-purpose STORage (MAGNASTOR). The objective of this study was to develop models and perform thermal analyses using best estimate data provided by the utility, Duke Energy, fuel assembly design information provided by the fuel vendors, Westinghouse Electric Company and AREVA, and decay heat estimates for each fuel rod from Oak Ridge National Laboratory (ORNL) based on actual power history data.

Detailed models of the NAC MAGNASTOR were developed using two codes, COBRA-SFS (Michener et al. 2015) and STAR-CCM+[1] (CD-adapco 2015). The immediate purpose of this modeling effort was to obtain temperature predictions for a loaded fuel storage cask in the Catawba Nuclear Station ISFSI. Estimates of fuel cladding temperatures were of primary interest, but temperatures of the cask components were captured as well. The models developed for both codes represent the entire cask, but the capabilities of each code are exploited to capture detailed evaluations of different portions of the system. COBRA-SFS is used to model the fuel and basket region in detail and provide an accurate representation of heat transfer by radiation, convection, and conduction in the radial direction from the fuel to external ambient. Heat transfer paths through the base and top of the cask, which are by design of much lesser significance compared to radial heat removal, are treated in a more simplistic manner. STAR-CCM+ is used to model the solid structures of the basket and concrete cask in detail, including the base and lid regions, but approximates the fuel assemblies within the basket as a porous media, and utilizes an effective thermal conductivity model to capture fuel cladding temperatures. With consistent material specifications and the same boundary conditions, these two models are complementary and provide an effective consistency check to verify that the models are appropriately capturing the physical behavior of the system. This provides some confidence that the results of the thermal evaluations accurately represent the temperatures that will be achieved in the storage system, within the uncertainty in the various input parameters provided.

Except for assumptions regarding ambient boundary conditions, the models produced for this study can be considered "best estimate". They omit many of the conservatisms and bounding assumptions normally used in design-basis and safety-basis calculations for spent fuel storage systems. The models include pin-by-pin decay heats based on burnup data provided by Duke

[1] STAR-CCM+ is a commercial CFD software product of CD-adapco.

Energy, under a non-disclosure agreement (NDA). The COBRA-SFS model also includes fuel geometry provided by the fuel vendors under NDA.

Fuel cladding temperatures are of interest when they at their highest, during initial loading and installation in the ISFSI, and as they cool over potentially extended storage times. For that reason, decay heat values were calculated and used to estimate corresponding fuel cladding temperatures for the time of loading and for 10, 50, 100, 200, and 300 years of storage.

Ambient conditions are the same used in the Final Safety Analysis Report (FSAR) (NAC 2011), which consisted of a 24°C (76°F) ambient with regulatory levels of solar insolation. This is representative of the mean ambient temperature at the Catawba Nuclear Station site during August of 2014. Two additional COBRA-SFS runs were completed with a 38°C (100°F) ambient, with and without solar insolation, for comparison with cladding temperatures estimated for the TN-32B in Fort et al. (2016).

Estimates of cladding temperature during the vacuum drying process were also of interest; in particular, the peak cladding temperature (PCT) that could have occurred during the vacuum drying process, for comparison to PCT under steady-state conditions when the storage system was placed in the ISFSI. Using canister vacuum drying records provided by Duke Energy, the vacuum drying transient was calculated. The COBRA-SFS model that was developed for storage steady-state thermal analysis was used for this transient simulation after incorporating appropriate boundary and initial conditions.

General background for the NAC MAGNASTOR and specific information relative to the selected canister and cask at the Catawba Nuclear Station are provided in Section 2.0. Best estimate decay heat values calculated by ORNL are provided in Section 3.0. The model constructed for COBRA-SFS is described in detail in Section 4.0. The STAR-CCM+ model is described in Section 5.0. Results obtained with the two models are presented in Sections 6.0 and 7.0. Section 8.0 lists the conclusions from this work, and Section 9.0 contains the list of references cited. Results using design basis loading and using decay heats as provided by Duke Energy are provided in Appendix A.

2.0 STORAGE MODULE

General information about the NAC MAGNASTOR is included in this section along with information about the storage site.

2.1 Module Description and Thermal Characteristics

The MAGNASTOR is a spent nuclear fuel dry storage system manufactured by NAC International, Inc. The MAGNASTOR has a fuel storage canister inside of a ventilated concrete cask. NAC refers to their canister as the transportable storage canister (TSC).

An external view of the MAGNASTOR is shown in Figure 2-1. The concrete cask inner cavity and air flow passages are lined with carbon steel plate. The TSC sits on an elevated pedestal above the four air inlets. At the ground level, each of the inlet passages are partially filled with several rows of vertical, cylindrical pins that provide shielding. Radial positioning of the TSC within the concrete cask cavity is maintained by carbon steel standoff supports that extend outward from the concrete cask inner shell. Outlet air passages and vents are included near the top of the concrete cask. Access to the inner cavity for insertion of the TSC is provided by a removable lid.

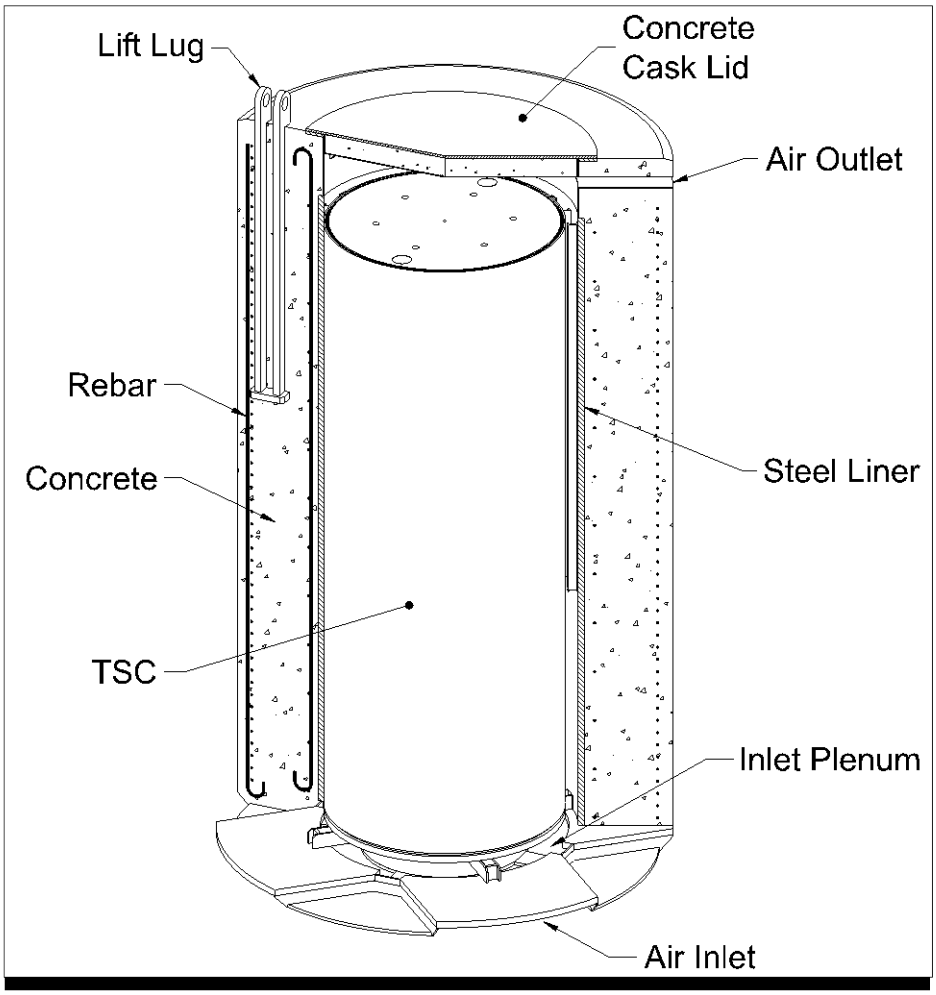

Figure 2-1. MAGNASTOR Storage System

The TSC shell and pressurized water reactor (PWR) fuel basket is shown in Figure 2-2. The basket has 37 assembly positions for PWR fuel, as is used at Duke Energy's Catawba Nuclear Station. An alternate design has 87 assembly positions for boiling water reactor (BWR) fuel. The fuel tubes are made from carbon steel plate and are connected to adjacent tubes at the corners by machined rods. Neutron absorbers are attached to the fuel tube walls with a thin stainless steel retainer on the outer face. Carbon steel side and corner support assemblies are bolted to the basket assembly and position the assembly within the TSC. The TSC shell and bottom are manufactured using stainless steel, as is the TSC lid. The TSC lid shield material is carbon steel.

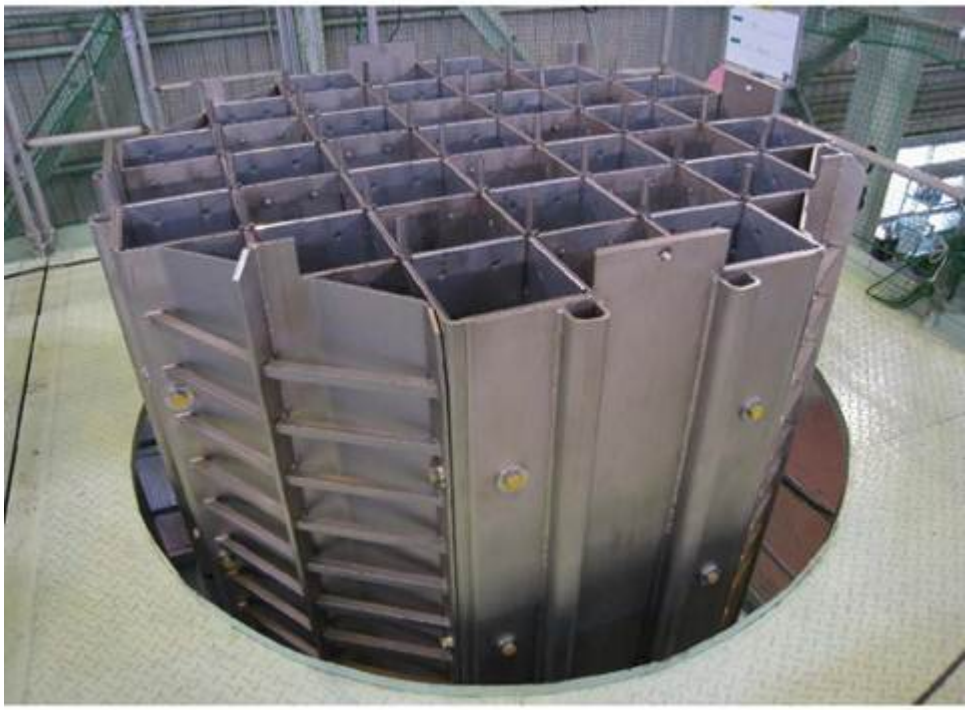

Figure 2-2. MAGNASTOR PWR Basket

In normal operations, the loaded TSC is moved from the transfer cask into the concrete cask following vacuum drying and backfill with helium. The assembled storage system is then transported by crawler transport to the ISFSI.

2.2 Installation at Duke Energy's Catawba Nuclear Station

This section describes the site location and the canister selected for analysis.

2.2.1 Site Location

The Catawba Nuclear Station is located on a peninsula on Lake Wylie, which is on the Catawba River, about 18 miles south of Charlotte, North Carolina. A satellite view of the plant is shown in Figure 2-3.

Figure 2-3. Satellite View of Duke Energy's Catawba Nuclear Station

2.2.2 Selected Canister and Loading

The canister selected for this analysis is CNZ-078. This canister was loaded in August, 2014. Two fuel types are included in this loading, MkBW and W-RFA. MkBW is Areva 17x17 fuel and W-RFA is Westinghouse 17x17 fuel.

Unfortunately, due to proprietary concerns this is all that can be shared about the canister loading. Best estimate calculated values of decay heat are discussed in Section 3.0.

3.0 DECAY HEAT ESTIMATES

Estimates of assembly decay heat were calculated by ORNL based on the pin-by-pin burnup data provided by Duke Energy. The calculations of decay heat were done with the ORIGAMI[2] tool from SCALE 6.2 (Rearden and Jessee, 2016) that is an ORIGEN super sequence developed for light water reactor fuel analysis. These calculations were done in a similar way as those for the North Anna fuel for the TN-32B thermal models (Fort et al. 2016). However, since less data was provided by the utility than in the North Anna case, the methodology was adjusted and instead of creating cross-sections with TRITON[3] for every node of each assembly, assemblies were grouped depending on their fuel type and reactor history (i.e., burnable absorbers, boron concentration, etc.). For the components inside the fuel, it was assumed that only the cobalt was activated. That is the only significant contributor to decay heat for the time scales of interest. The cobalt mass for each component was assumed conservatively since that information was not available.

ORIGEN has been validated against Swedish calorimetric measurements of spent fuel assemblies and has a standard deviation of less than 2% for PWR assemblies, which is typically the uncertainty in burnup. Burnup is the main driver of decay heat.

Results of these calculations included pin-by-pin decay heats for each assembly. The results are referred to in this report as "best estimate" values and were computed for initial loading and at 10, 50, 100, 200, and 300 years after loading. Note that the loading map provided by Duke Energy specified the earliest loading date in July 2014 and this was the month and year used when computing decay heat values. After these calculations were completed, actual loading dates observed in vacuum drying records (see Table 6-1) were during August 2014. Therefore, estimated decay heat values will be slightly higher than on the date of actual loading. To avoid confusion, August 2014 will be used throughout this report as the date for initial canister loading and for decay heat values at initial loading.

After a description of assumptions regarding axial decay heat profile in Section 3.1, the aggregated totals of decay heat for each assembly are reported in Section 3.2 for their respective position within the TSC basket.

3.1 Axial Decay Heat Profiles

Since no information was provided upon which to base axial decay heat profiles for the loaded fuel assemblies, ORNL instead used a database containing approximately 3000 burnup profiles from different reactors. From that database, a subset using similar reactors, initial enrichment and burnup resulted in an average profile that was used for the assemblies. The impact of different

[2] Source terms and spent nuclear fuel (SNF) storage pool decay heat load analyses for operating nuclear power plants require a large number of Oak Ridge Isotope Generation and Depletion (ORIGEN) calculations. SNF source term calculations also require a significant amount of bookkeeping to track quantities such as core and assembly operating histories, spent fuel pool resident times, heavy metal masses and enrichments. The ORIGEN Assembly Isotopics (ORIGAMI) module in the SCALE code system provides a simple scheme for entering these data (Wieselquist et al. 2016).

[3] See http://scale.ornl.gov/overview/triton.htm.

burnup profiles on the assembly average decay heat is less than half a percent. It does, however, have a significant impact on the axial distribution of decay heat.

The axial decay heat profiles for each assembly, for input to the thermal models, were constructed by Pacific Northwest National Laboratory (PNNL) from the pin-by-pin decay heat data. The resulting axial decay heat profiles are shown in Figure 3-1. The profiles are essentially the same for all assemblies. Figure 3-1 also shows the standard axial profile for low-burnup fuels from DOE-RW-0472 (DOE 1997). This profile was used in the initial thermal model calculations in Appendix A for design basis loading and for the conservative decay heat values provided by the utility.

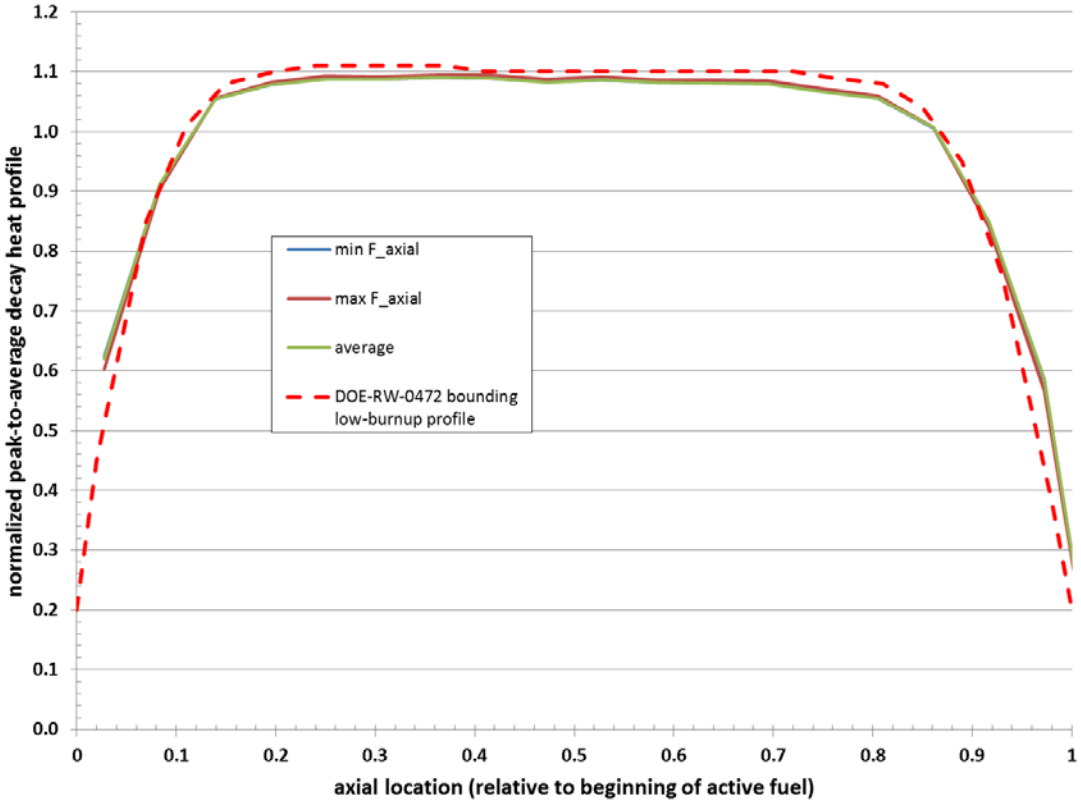

Figure 3-1. Maximum, Minimum, and Average Axial Profiles Compared with the Standard Axial Profile for Low-Burnup Fuels (DOE 1998)

3.2 Assembly Decay Heat Values

Assembly decay heat estimates at the time of the initial loading (August 2014) are shown in Figure 3-2. Assembly decay heat values estimated for future dates are shown in Figure 3-3 through Figure 3-7. These include dates of 10, 50, 100, 200, and 300 years after loading.

		626.66	620.82	423.84		
	630.54	854.37	796.00	854.67	413.78	
661.31	850.57	784.67	751.95	703.88	818.99	664.12
663.32	846.64	754.10	757.81	697.24	819.21	683.34
675.28	833.97	769.34	697.44	882.76	854.37	672.24
	416.89	867.83	802.50	892.98	647.53	
		415.35	661.95	646.74		

Figure 3-2. Best Estimate Assembly Decay Heats for Initial Loading (W)

		503.35	502.24	351.81		
	503.88	617.57	629.05	617.73	340.50	
535.75	626.87	607.44	568.90	562.28	651.00	536.51
535.74	626.56	571.55	571.89	559.05	650.78	546.25
543.62	617.59	571.28	559.12	576.18	637.58	546.59
	345.52	627.17	640.00	621.71	522.79	
		344.87	536.04	522.20		

Figure 3-3. Best Estimate Assembly Decay Heats after 10 Years (W)

		273.34	272.71	197.82		
	271.44	326.82	331.99	326.90	190.08	
288.98	331.13	324.45	306.75	302.36	342.40	289.48
288.98	330.96	308.24	308.42	301.60	342.32	292.56
291.18	326.83	307.22	301.63	308.88	335.97	292.75
	194.35	331.30	338.16	327.18	279.61	
		194.00	289.17	279.31		

Figure 3-4. Best Estimate Assembly Decay Heats after 50 Years (W)

		162.15	161.77	121.62		
	159.69	188.94	191.84	188.98	115.92	
171.65	191.20	190.14	180.59	177.92	199.81	171.97
171.65	191.11	181.48	181.58	178.13	199.76	171.55
170.77	188.94	180.87	178.15	181.44	193.70	171.66
	119.48	191.30	197.38	188.20	164.54	
		119.27	171.77	164.37		

Figure 3-5. Best Estimate Assembly Decay Heats after 100 Years (W)

		97.88	97.64	77.72		
	96.82	111.62	113.11	111.64	73.75	
104.24	112.78	114.09	108.26	105.45	117.26	104.45
104.24	112.73	108.67	108.73	106.15	117.22	103.30
102.85	111.62	108.43	106.16	107.30	114.04	103.35
	76.37	112.84	115.62	110.76	99.36	
		76.25	104.33	99.25		

Figure 3-6. Best Estimate Assembly Decay Heats after 200 Years (W)

		76.88	76.69	63.07		
	76.90	87.43	88.38	87.45	59.96	
82.02	88.25	89.65	84.91	81.76	89.81	82.18
82.02	88.22	85.13	85.18	82.51	89.78	81.59
81.24	87.43	85.04	82.51	83.06	89.12	81.63
	62.01	88.30	88.53	86.82	78.31	
		61.91	82.09	78.22		

Figure 3-7. Best Estimate Assembly Decay Heats after 300 Years (W)

4.0 COBRA-SFS MODEL DESCRIPTION

Section 4.1 describes the representation of the solid material components of the storage system, and Section 4.2 presents a detailed discussion of the rod-and-subchannel representation of the fuel assemblies within the basket.

4.1 Representation of MAGNASTOR for COBRA-SFS

A schematic diagram of the MAGNASTOR is shown in Figure 4-1, which also identifies the basic elements of the COBRA-SFS model of this system. The major path of heat removal from the fuel assemblies in the TSC (and all canister types in vertical storage systems in general) is in the radial direction, by conduction, convection and thermal radiation. Heat is removed from the canister's exterior surface by convection to the buoyancy-driven airflow in the annulus between the concrete cask and TSC shell. Thermal radiation is also significant in carrying heat from the canister to the concrete cask liner and lid, where it is either removed by convection to the cooling airflow or transferred to the outer surfaces of the concrete cask by conduction. From there it is dissipated to the environment by convection or thermal radiation to the essentially infinite heat sink of the ambient air. Heat can also leave the system through the lid structures and base of the cask, but this is generally an insignificant path compared to the radial pathway. For an air-cooled system such as the MAGNASTOR, the majority of the heat is carried out by the air flow in the annulus.

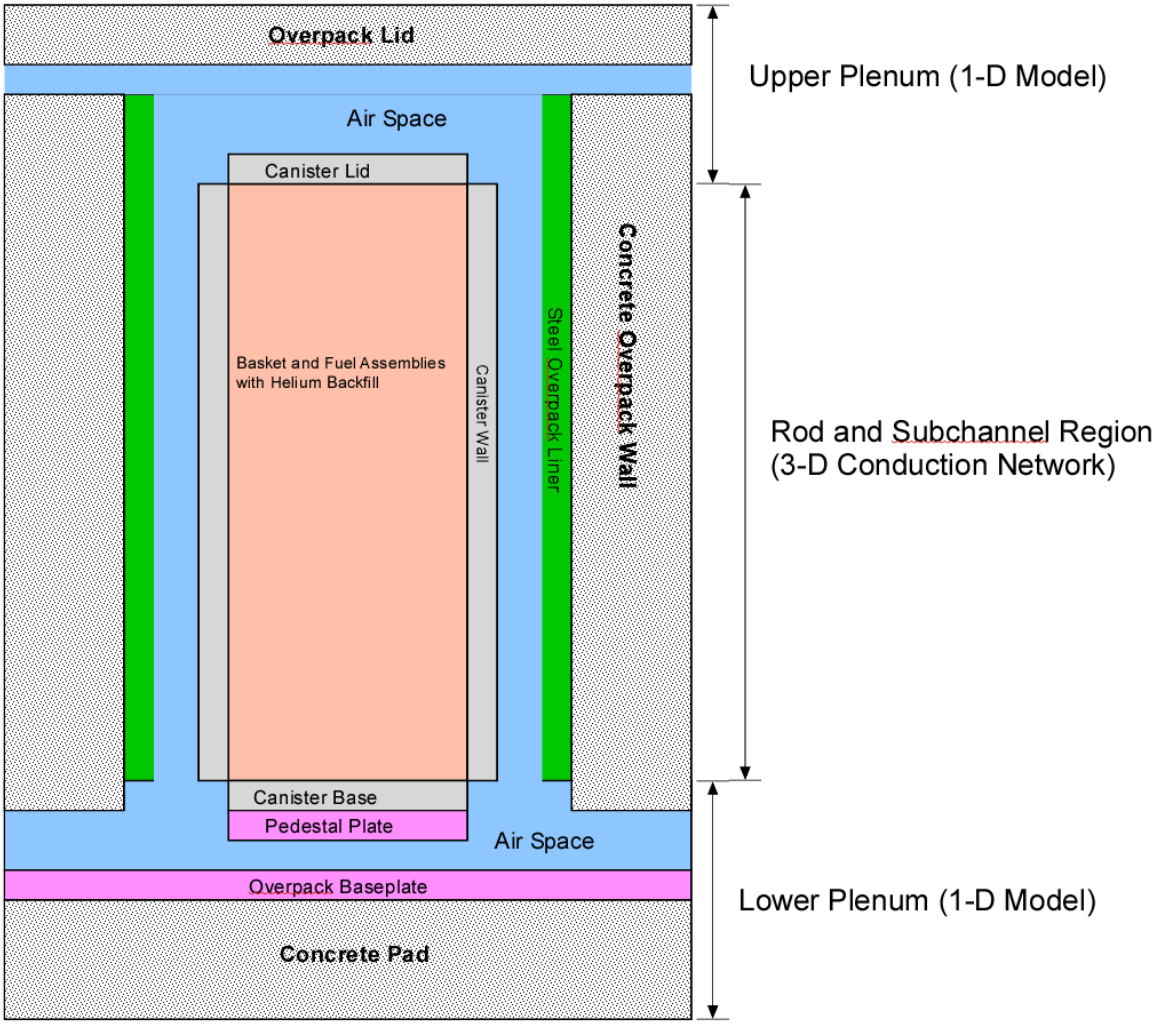

Figure 4-1. Diagram of MAGNASTOR Showing Major COBRA-SFS Model Regions (NOTE: model image not to scale)

Consistent with the significant heat transfer paths in the system, the COBRA-SFS modeling approach provides a detailed, highly resolved representation of the fuel assemblies, basket plates, support assemblies, and canister shell over the axial length of the basket. This allows the model to appropriately represent heat transfer by conduction, convection, and thermal radiation in the region of most significant heat removal, to obtain accurate and physically meaningful predictions of local component temperatures, including detailed temperatures and temperature distributions for the fuel rods within the assemblies. Axial heat transfer paths from the system, which in most configurations consists of conduction through layered solid structures, are represented with a network of locally one-dimensional heat transfer paths, using appropriate material properties and contact resistances for the layered components.

Diagrams illustrating the detailed 3-D solid conduction network for the COBRA-SFS model representation of the basket, supports, TSC shell, and concrete cask are shown in Figure 4-2 and Figure 4-3. These diagrams are not to scale, with nodal thicknesses greatly exaggerated for clarity. Figure 4-2 focuses on the representation of the radial heat transfer paths through the

basket, basket supports, and canister shell, to the cooling air flow in the annulus between the TSC and concrete cask inner wall. The basket cells are formed by carbon steel plates, while the neutron absorber is assumed to be composed of equal thickness layers[4] of aluminum and neutron absorber composite with a thin stainless steel retainer on the outer face. These layered components are attached to the basket structure with steel weld posts. However these fine details were not represented in the model.

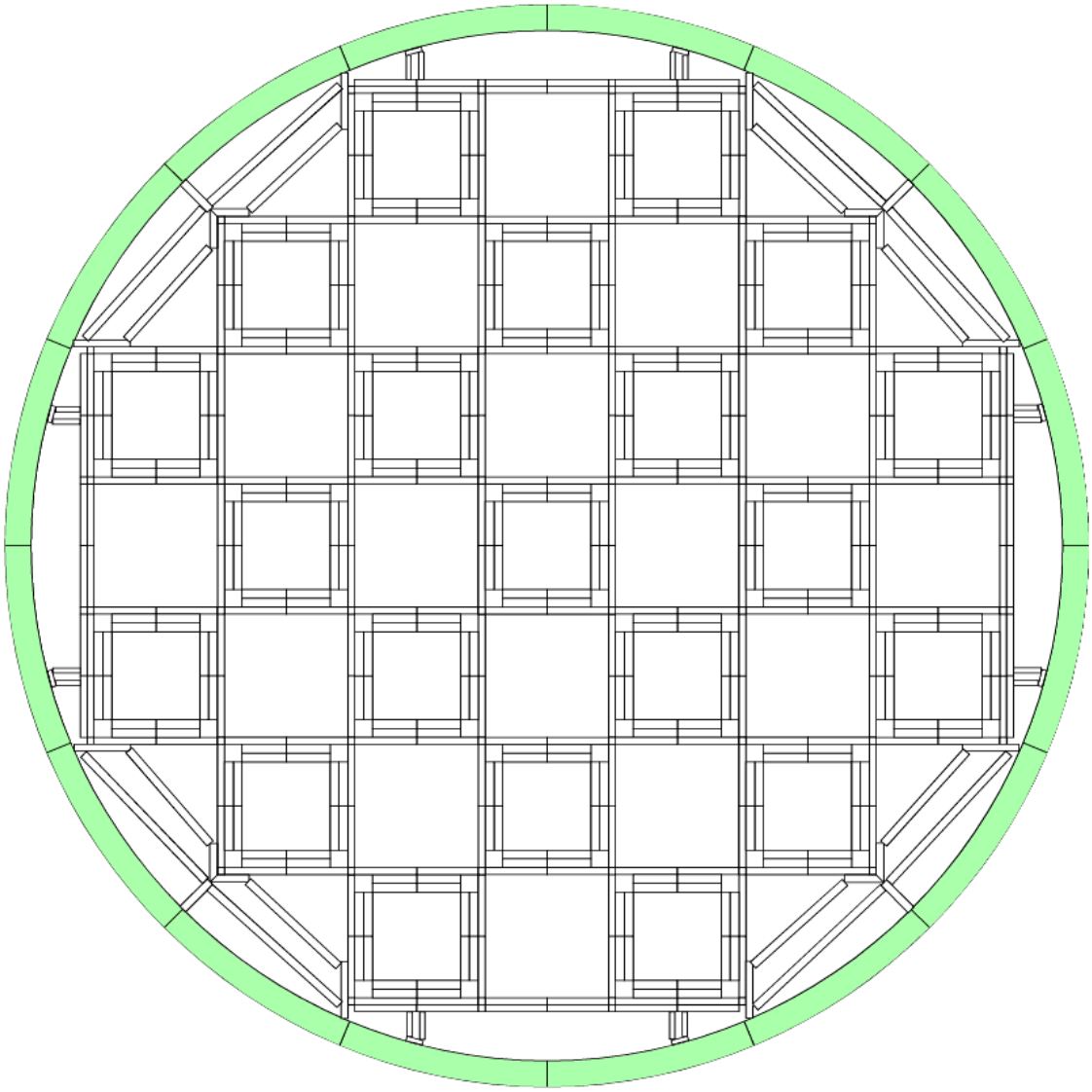

Figure 4-2. Diagram of COBRA-SFS Model of MAGNASTOR TSC Cross-Section Illustrating TSC Shell, Basket and Support Rail Nodalization
(NOTE: diagram not to scale; node thicknesses greatly exaggerated for clarity)

[4] This assumption was made after considering ambiguous information in engineering drawings. Corrected description follows.

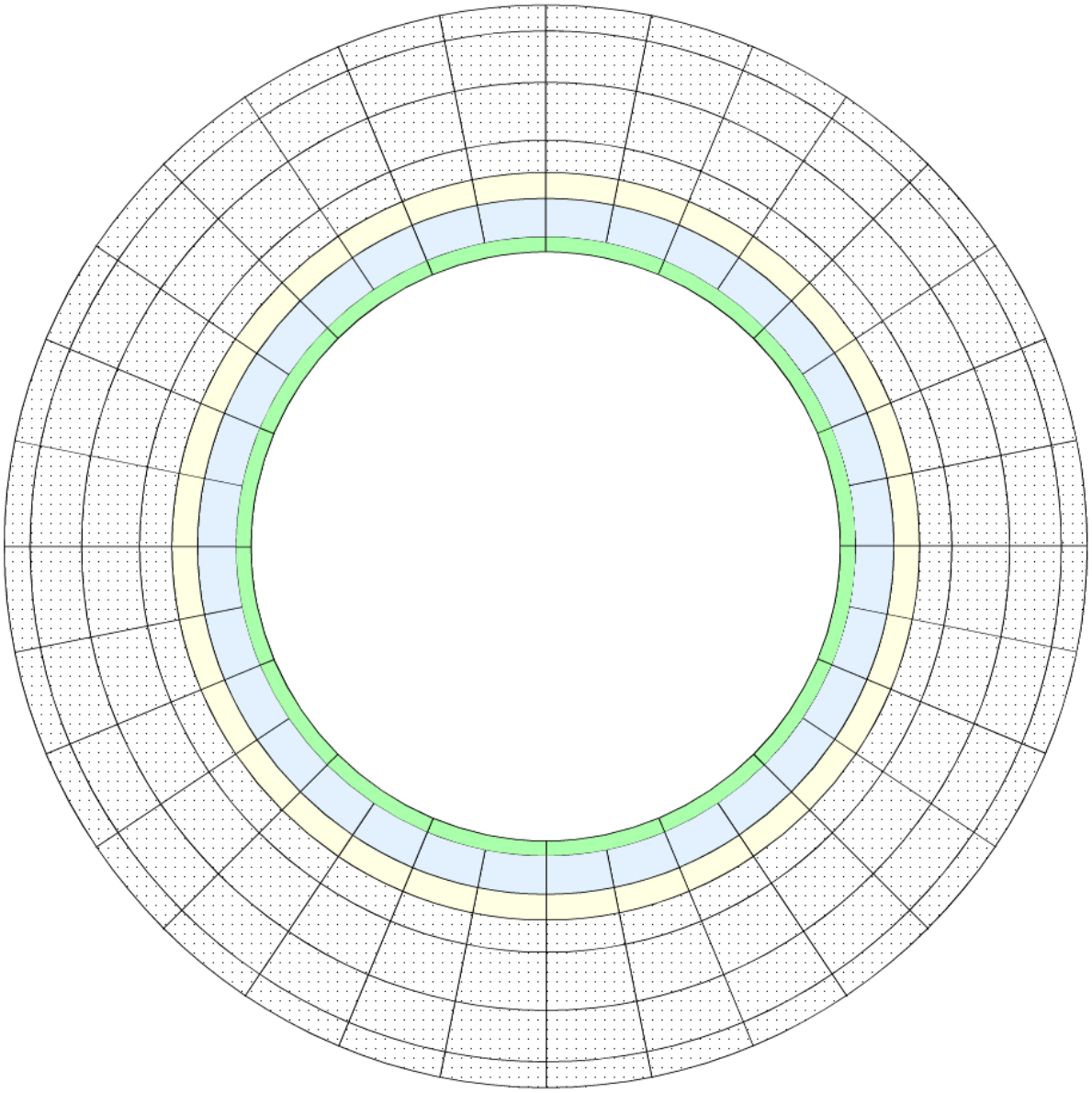

Figure 4-3. Diagram of COBRA-SFS Model of MAGNASTOR Concrete Cask Cross-Section Illustrating Nodalization of Overpack Body and Exterior Surface (NOTE: diagram not to scale; node thicknesses greatly exaggerated for clarity)

Thermal gap resistances are included with the neutron absorber because of the imperfect contact between adjacent layers and the consequent effect on contact conductance, since the plates are fastened together only at intermittent points, and because the two materials have different coefficients of thermal expansion. The COBRA-SFS model assumes a resistance equivalent to a 0.01-inch gap between the fuel tube and neutron absorber and between the neutron absorber and the retainer. Heat transfer across each gap is assumed to consist of conduction through helium gas filling the gap and thermal radiation between the adjacent flat plates.

Note that following completion of this analysis, Duke Energy reviewers provided a corrected description of the neutron absorbers[5]. Instead of separate layers of neutron absorber composite and aluminum, which would presumably have a thermal gap resistance between them, these are in fact a one-piece construction consisting of an inner core of compacted aluminum and boron carbine powders clad in much thinner aluminum plating. However, because of the high thermal conductivity of the aluminum and the neutron absorber composite and because a gap resistance was not incorporated between them in the model, the difference in thermal resistance between the assumed and the actual geometry is not significant.

The carbon steel support assemblies between the sides and corners of the basket and the inner surface of the TSC shell are modeled as shown in Figure 4-2. In the MAGNASTOR, these supports are fastened to the basket with bolts (used as screws) at intermittent locations along the axial length of the basket. Since the basket and supports are made of the same material, a gap resistance is not imposed at this interface. However a gap resistance is imposed between each of the corner supports and the TSC shell equivalent to 0.3 inches of helium.

As shown by the diagram in Figure 4-3, the noding for the COBRA-SFS model becomes much simpler for the concrete cask body, in keeping with the much simpler geometry and direct radial heat transfer paths through the layered steel shells of the cask. The noding mesh for the cask shell is divided into segments encompassing 22.5° of arc, which is more than adequate to provide a reasonable interface with the detailed modeling of the cask internal structure, as illustrated in Figure 4-2. The somewhat less detailed azimuthal resolution of the cask shell in the modeling is sufficient to capture the modest asymmetry in the fuel loading pattern used for the canister (as shown in Section 3.2). The thin carbon steel inner liner is represented with a thickness of one node. The thick concrete layer comprising the body of the concrete cask is represented with four layers of variable thickness nodes. Comparison with temperature gradients obtained in the more detailed mesh of the STAR-CCM+ model show that this is more than sufficient to capture the radial and circumferential gradients in the thick metal and concrete layers of the cask structure.

4.2 Representation of Fuel Assemblies and Internal Convection in the COBRA-SFS Model

The fuel assemblies within each of the 37 cells in the MAGNASTOR basket are represented in the COBRA-SFS model using rod-and-subchannel modeling of the actual assembly geometry. This approach uses a representation of the fluid flow and heat transfer paths within the rod array that was originally developed for analysis of core hydrodynamics in operating reactors, and is still in use today in reactor core and primary system modeling software. The original reactor core code was later expanded and extended to be applicable to computational fluid and thermal analysis of spent fuel assemblies in dry storage packages, primarily by adding a detailed rod-to-

[5] From comments provided on draft report in September 13, 2016 email from Steve Nesbit (Duke Energy) to Brady Hanson, "MAGNASTOR thermal model report review".

rod and rod-to-wall thermal radiation modeling capability (see the COBRA-SFS documentation[6], Michener et al. 1995 and 2015, for full details).

A diagram of the basic rod-and-subchannel array for a 17x17 assembly is shown in Figure 4-4. (This diagram is not to scale; the gaps between the rods are greatly exaggerated for clarity.) This diagram is a generic illustration of the rod-and-subchannel modeling for a fuel assembly of this type, and does not show local variations due to control rod guide sleeves, instrument tube(s), or burnable poison rods. However, the COBRA-SFS model is capable of taking into account these individual variations in specific fuel assembly designs, and these variations in the specific assemblies were included in the modeled detail for both the Westinghouse Electric Company W-RFA and the AREVA MkBW fuel assemblies. Each assembly has 24 control rod guide tubes.

A unique feature of the COBRA-SFS code is the detailed modeling of the flow field within the fuel assemblies within the individual basket cells, accounting for local heat transfer by conduction and convection. Thermal radiation is also calculated directly, using grey-body view factors (rod-to-rod and rod-to-wall) for all rods in the array. This representation of the fuel assembly allows for a much more accurate resolution of the local gas temperatures and velocities, fuel cladding surface temperatures, and rod internal temperatures, compared to the typical approach used in computational fluid dynamics (CFD) and finite element analysis codes. In CFD codes, the assembly is typically modeled as a porous medium, and in CFD and finite element analysis codes, thermal radiation and conduction heat transfer within the fuel assembly is typically represented as a homogeneous block, using an effective conductivity model. Such an approach is described for the STAR-CCM+ model in Section 5.3.

[6] Cycle 4 of the COBRA-SFS code, which was used for the work reported here, has been released to the Radiation Safety Information Computational Center (RSICC) as of October 2015. It is available to the public, and includes complete documentation in electronic format.

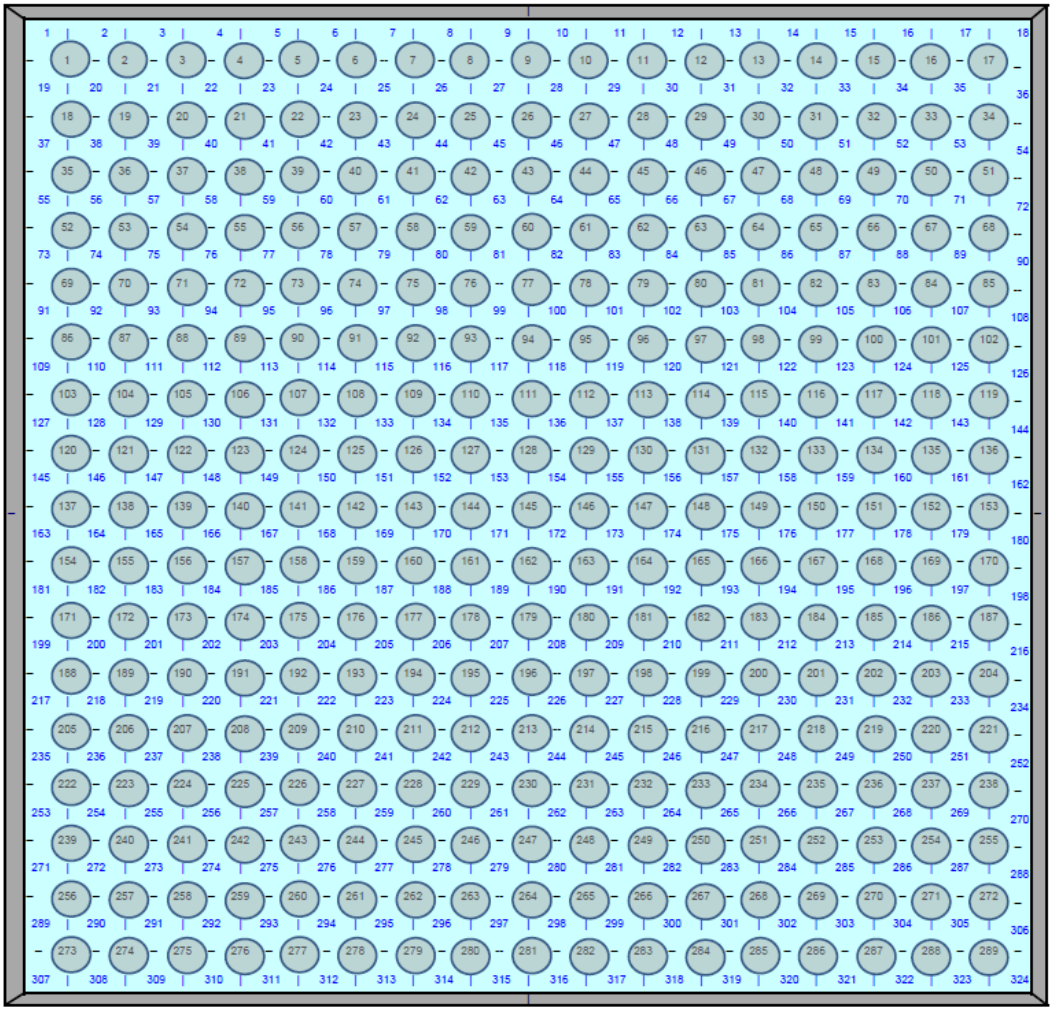

Figure 4-4. Rod-and-Subchannel Array Diagram for COBRA-SFS Model of 17x17 Fuel Assemblies within Basket Cells
(NOTE: diagram is not to scale)

For fluid convection within the system, heat transfer is represented with a user-specified heat transfer correlation. Based on validation of the COBRA-SFS code with experimental data from horizontal and vertical test systems and canisters loaded with actual spent fuel, convection is represented with the venerable Dittus-Boelter heat transfer correlation for turbulent flow,

$$Nu = 0.023(Re^{0.8})(Pr^{0.4})$$

where

Nu = Nusselt number
Re = Reynolds number, based on subchannel hydraulic diameter
Pr = Prandtl number for the backfill gas

For laminar flow conditions, a Nusselt number of 3.66 has been verified as applicable to spent fuel rod arrays (Lombardo et al. 1986; Michener et al. 1995; Rector and Michener 1989). In the COBRA-SFS code, the local heat transfer coefficient is defined as the maximum of the values calculated from the laminar and turbulent correlations specified by user input. Figure 4-5 illustrates the convenient mathematical behavior of these correlations as a function of Reynolds number.

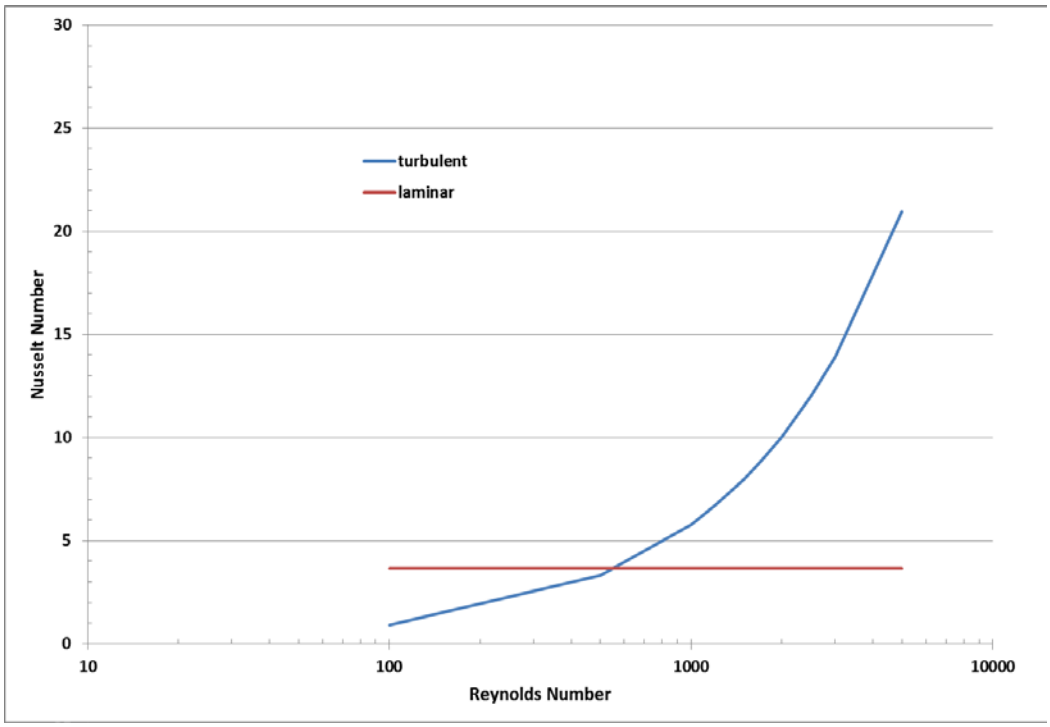

Figure 4-5. Laminar and Turbulent Formulations for Nusselt Number

The open regions of the support rails, as illustrated in the diagram in Figure 4-2, are represented as gas flow channels that allow a thermo-siphon natural convection recirculation within the cavity, with helium gas rising through the fuel assemblies within the basket, absorbing heat from the fuel rods, then mixing in the narrow head space above the basket and sinking down the open channels in the support rails, as heat is transferred from the gas to the cooler steel wall of the canister.

4.3 Material Properties

Well-tested values were used for properties of solids and gases. Specific treatment of density for the helium fill gas is described below.

4.3.1 Helium Fill Gas

For vertical storage systems, pressurized canisters offer significant improvements in convection heat transfer over non-pressurized systems due to the increase in gas density and associated heat

carrying capacity of the greater mass of fluid being recirculated within the fuel arrays. The advantage is far less in horizontal systems due to the shorter length scale and barriers to flow.

The COBRA-SFS steady-state thermal predictions were based on a helium gas pressure of 7 atm in the canister. This is consistent with the 83.02 psig (6.65 atm) fill gas pressure recorded during the vacuum drying and backfill process for canister CNZ-078, as long as the bulk gas temperature is reasonably close to the same value in storage as it is when that fill pressure was measured. As will be shown in Section 6.1.2, the PCT at the end of vacuum drying only differs from the value estimated for initial storage by 4°C. This suggests that the 7 atm gas pressure is a reasonable value for initial storage.

Simulations were also performed for reduced decay heat levels calculated for 10, 50, 100, 200, and 300 years of storage (Section 3.2). At these lower decay heat levels the system temperatures will be reduced and the gas pressure will be correspondingly lower. Since the average fill gas density remains the same (assuming no helium loss from the welded canister), this is not associated with any reduction in the potential for convective heat transfer. However, since COBRA-SFS uses a temperature dependent density for a specific pressure as input, the fact that the relationship for 7 atm was used for all storage times meant that an elevated helium density was used at longer storage times. This is illustrated in Figure 4-6.

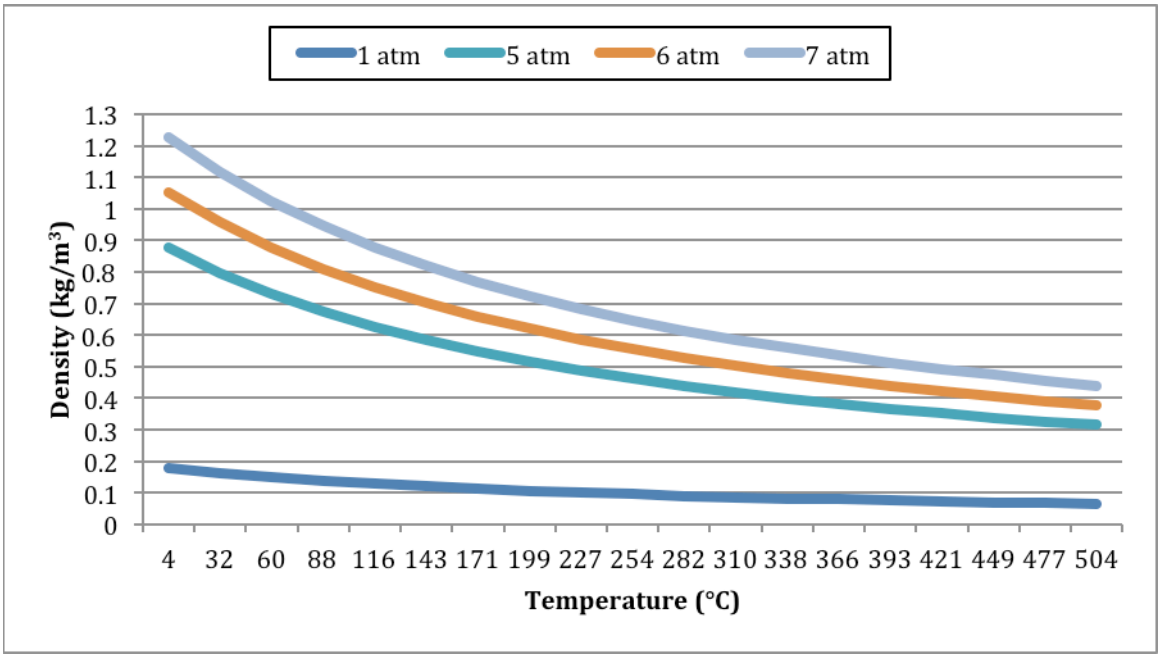

Figure 4-6. Density as a Function of Temperature for Helium

A sensitivity study was performed to determine the impact of correcting gas thermal properties for the estimated actual pressure in the cask at 100 and 300 years of storage. Using the thermal loading from the 300 year case, additional simulations were performed with helium properties at 3 atm and 5 atm. Of the two cases, the 5 atm properties reflected the correct bulk density (within 3%) for an average helium gas temperature in the canister. At this pressurization, the PCT was ~7°F (3.9°C) higher than the base assumption of 7 atm pressurization in the cask. A similar

check was made for the 100 year thermal loading simulation. In this case a simulation was performed for 6 atm of helium in the canister. The bulk density was still too high at 6 atm, and based on the density table for 5 and 6 atm, we can estimate the correct pressure to be ~5.6 atm in the canister at 100 years, with an increased PCT of ~5°F (2.8°C).

Based on this sensitivity analysis it can be reasonably assumed that at the density specified, if the pressurization is modeled within 0.5 atm of the correct pressure, the change in predicted PCT will be less than ~10°F. This is partially due to the nature of the pressurization effect where increased heat rejection dramatically tapers off with increasing pressure above about 5 atm.

4.3.2 Surface Properties

For thermal radiation heat transfer, surface emissivity values of the basket tubes, and canister wall were estimated from standard material properties. Carbon steel components were specified with an emissivity of 0.8[7]. Stainless steel components were specified with an emissivity of 0.36. The external surface of the concrete cask was specified with an emissivity of 0.8 for thermal radiation to the environment, as it was assumed to be painted with a high emissivity paint. The fuel rod cladding surface emissivity was assumed to be 0.8, which is a typical realistic estimate for spent fuel rods. These surface emissivities are listed in Table 4-1.

Table 4-1. Surface Emissivities

Material	Emissivity
Carbon Steel	0.8
Concrete Cask	0.8
Fuel Cladding	0.8
304 Stainless Steel	0.36

4.4 Boundary Conditions

In many storage systems, design basis analysis assumes 100°F (37.8°C) as a bounding value for daily average temperature for normal conditions of storage. NAC uses 76°F (24.4°C) in the FSAR and this same value is used in calculations here. Site temperatures for the Catawba Nuclear Station were not available for this analysis, however this temperature is also consistent with August 2014 temperatures in York, South Carolina, which is about 20 miles to the southwest of the ISFSI, as reported by National Oceanic and Atmospheric Administration[8].

[7] As part of their review of this report, NAC International pointed out that the carbon steel basket and supports had electroless nickel coating and that the surface emissivity was considerably lower than the value shown here for uncoated carbon steel. A range of 0.2 to 0.32 is listed in the FSAR for surface emissivity of electroless nickel on mild steel. NAC uses 0.22 in their analysis, which is at the conservative end of this range. A sensitivity run was performed with COBRA-SFS to quantify the difference this would make for the best estimate case for initial loading. With the change in basket surface emissivity from 0.8 to 0.22 the peak cladding temperature was increased by 9°C (16°F).

[8] http://www.ncdc.noaa.gov.

Regulatory solar loading was included as shown in the 24 hour average values listed in Table 4-2.

Table 4-2. Solar Loading (10CFR71 2003)

Surface	Insolation over 24 hours (Btu/ft^2)	Insolation Rate ($Btu/hr\text{-}ft^2$)
Side	1475	61.46
Top	2950	122.92

A sensitivity study was performed with COBRA-SFS to determine the effect on PCT of different assumptions for ambient conditions. The first case used the same 76°F (24.4°C), but without any solar loading. The second case was for a 100°F (37.8°C) boundary temperature with solar loading. The results are shown in Table 4-3.

Table 4-3. Sensitivity of Storage PCT to Assumed Ambient Conditions - Initial Loading

Case	PCT, °F	PCT, °C
76°F (24.4°C) ambient, with solar	575.3	301.8
76°F (24.4°C) ambient, without solar	575.1	301.7
Difference	0.2	0.1
76°F (24.4°C) ambient, with solar	575.3	301.8
100°F (37.8°C) ambient, with solar	595.8	313.2
Difference	20.5	11.4

These results show that the addition of solar insolation has little effect on the PCT. The significant factor is the assumed air temperature. This result would be expected to be much different for a metal cask such as the TN-32B investigated in Fort et al. (2016). In a ventilated storage system like the MAGNASTOR, the canister temperature and the temperature of its contents is set primarily by the rate of heat transfer to the cooling airflow. Radiant heat transfer from the canister to the inner liner of the concrete cask is a secondary effect and the addition of solar loading on the outside of a thick-walled concrete cask produces little change in the liner temperature or the rate of heat transfer in the annulus.

The change in ambient temperature, however, directly impacts the sink temperature for heat transfer from the canister. The 24 °F (13.3 °C) change in ambient temperature results in an increase in PCT of similar magnitude, 20.5 °F (11.4 °C).

5.0 STAR-CCM+ MODEL DESCRIPTION

The present model was developed using STAR-CCM+, version 10.02, for all steps except definition of model geometry, which was performed with SolidWorks (Dassault Systemes 2011).

5.1 Model Geometry

The following sections describe the model geometry, which includes the 3-dimensional model and the mesh.

5.1.1 Geometry

A 3-dimensional model of the MAGNASTOR geometry was created in the solid modeling Computer Aided Design (CAD) software SolidWorks (Dassault 2011). The CAD geometry was generated from 2-dimensional drawings of the MAGNASTOR assembly provided by NAC. The CAD geometry is shown in Figure 5-1.

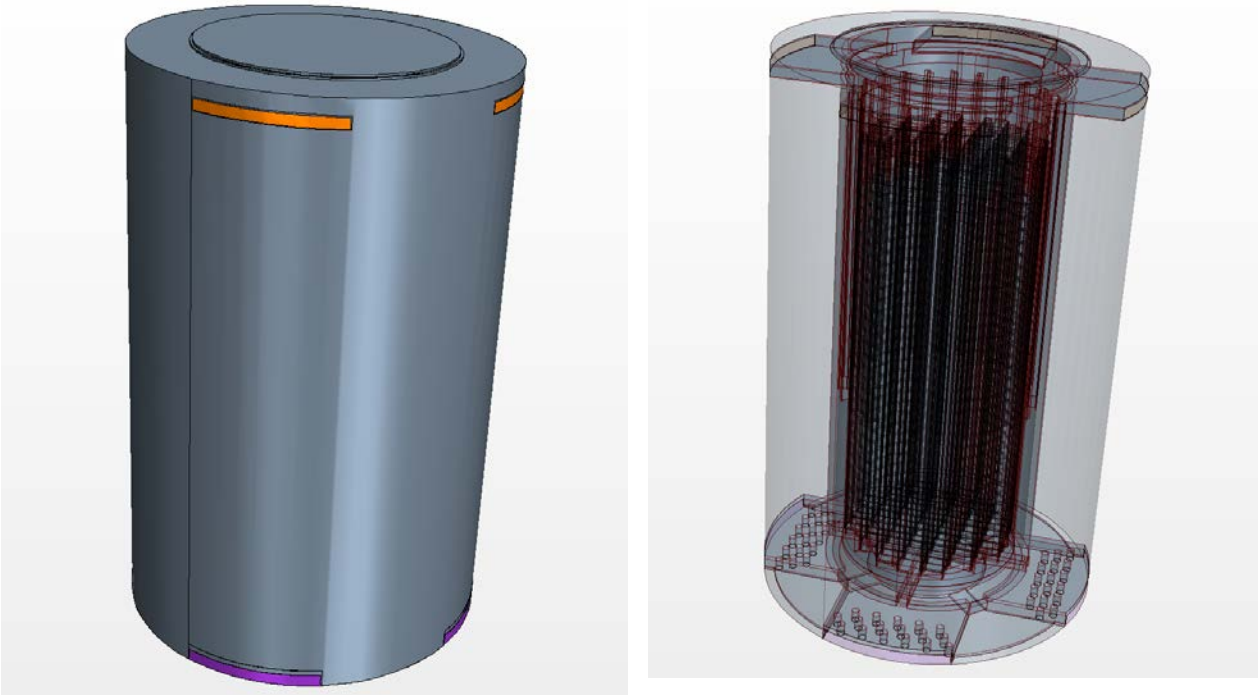

Figure 5-1. CAD Model Geometry for MAGNASTOR Assembly

5.1.2 Mesh

The SolidWorks geometry was imported into STAR-CCM+. The geometry was then meshed into 77 separate regions connected by 380 interface boundaries, resulting in a single conformal volume mesh across all regions. The polyhedral volume mesh contains 6,126,939 cells, 27,338,512 faces, and 21,361,006 vertices. Along each wall/fluid interface, the mesh contains a

prism layer to improve the accuracy of the flow solution near the walls. The prism layer consists of orthogonal prismatic cells, 4 cells thick, adjacent to the wall boundaries. Figures 5-4 through 5-6 show the mesh assembly.

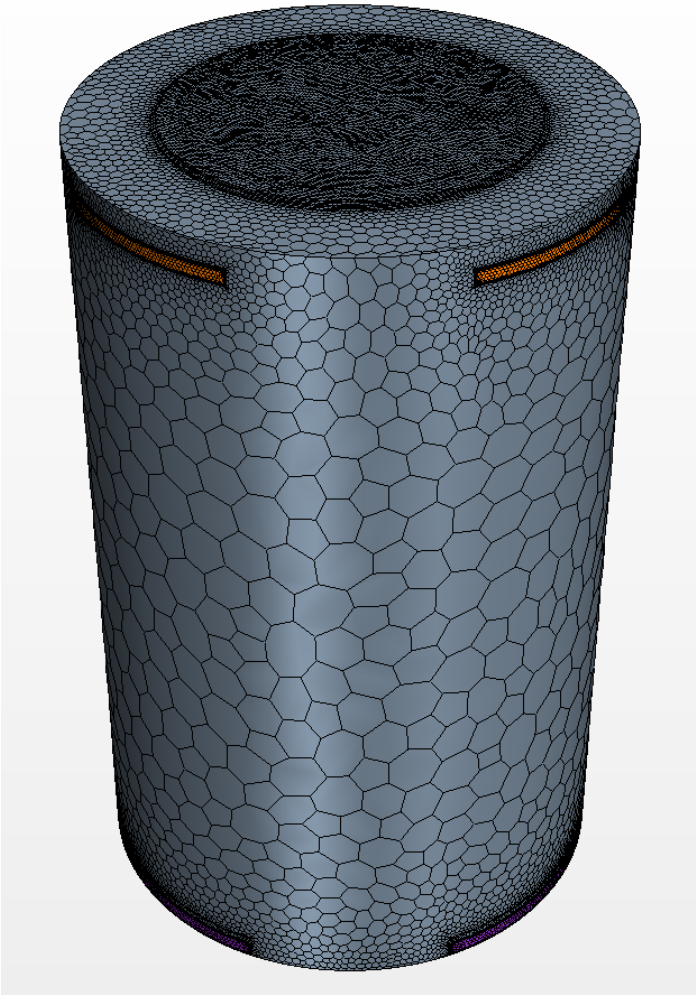

Figure 5-2. MAGNASTOR Assembly Mesh

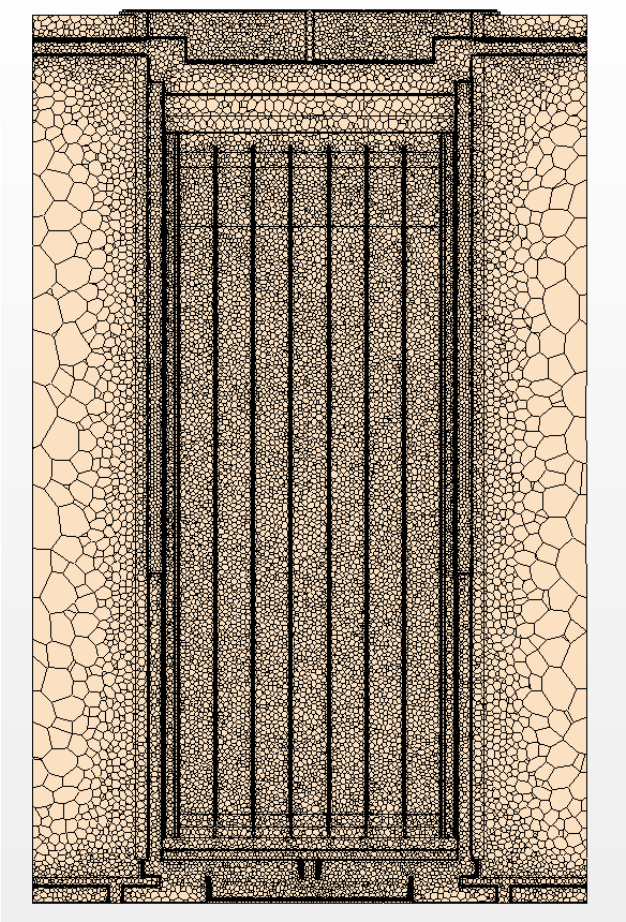

Figure 5-3. MAGNASTOR Assembly Mesh – Axial Cross-sectional View

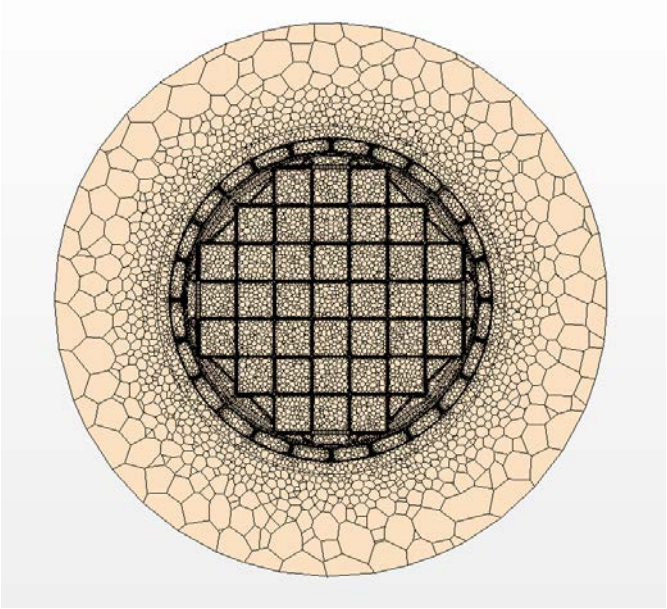

Figure 5-4. MAGNASTOR Assembly Mesh – Radial Cross-sectional View

A mesh sensitivity study was conducted to ensure proper mesh resolution. Five different simulations were run with representative inputs and meshes of varying resolution. The core poly mesh size ranged from 0.2-0.5 meters. Temperature results for the peak TSC shell and fuel assembly are shown in Figures 5-5 and 5-6. The plots show that the peak temperatures did not vary much with mesh resolution. Based on the results, a base mesh size of 0.5 meters was used for the MAGNASTOR simulation.

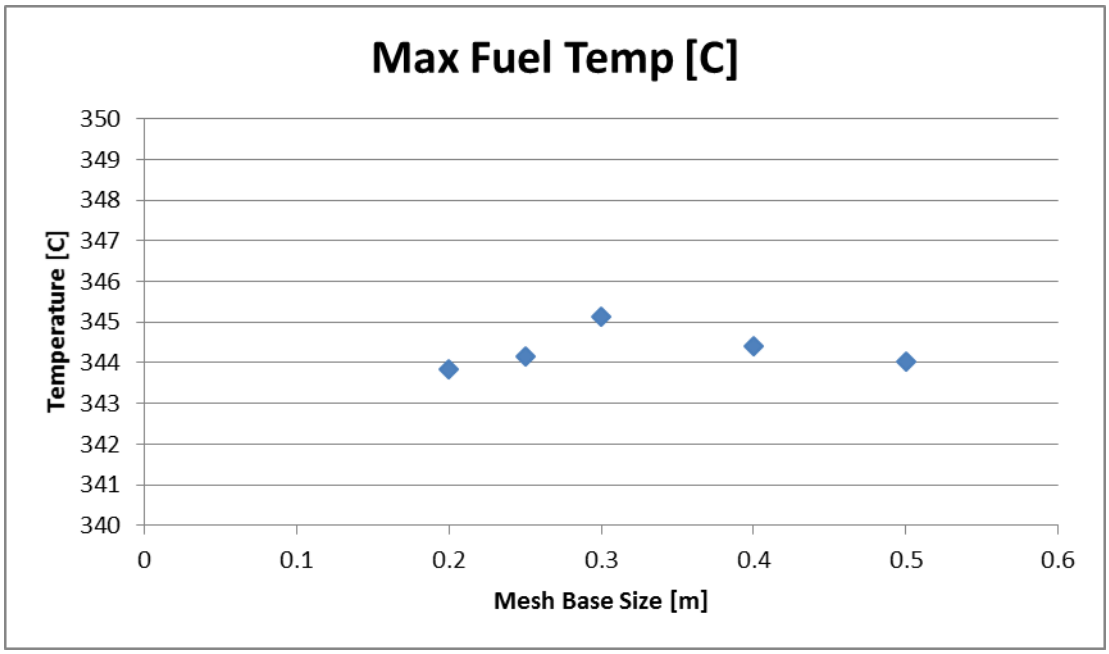

Figure 5-5. Mesh Sensitivity Study – Peak Fuel Assembly Temperature Results

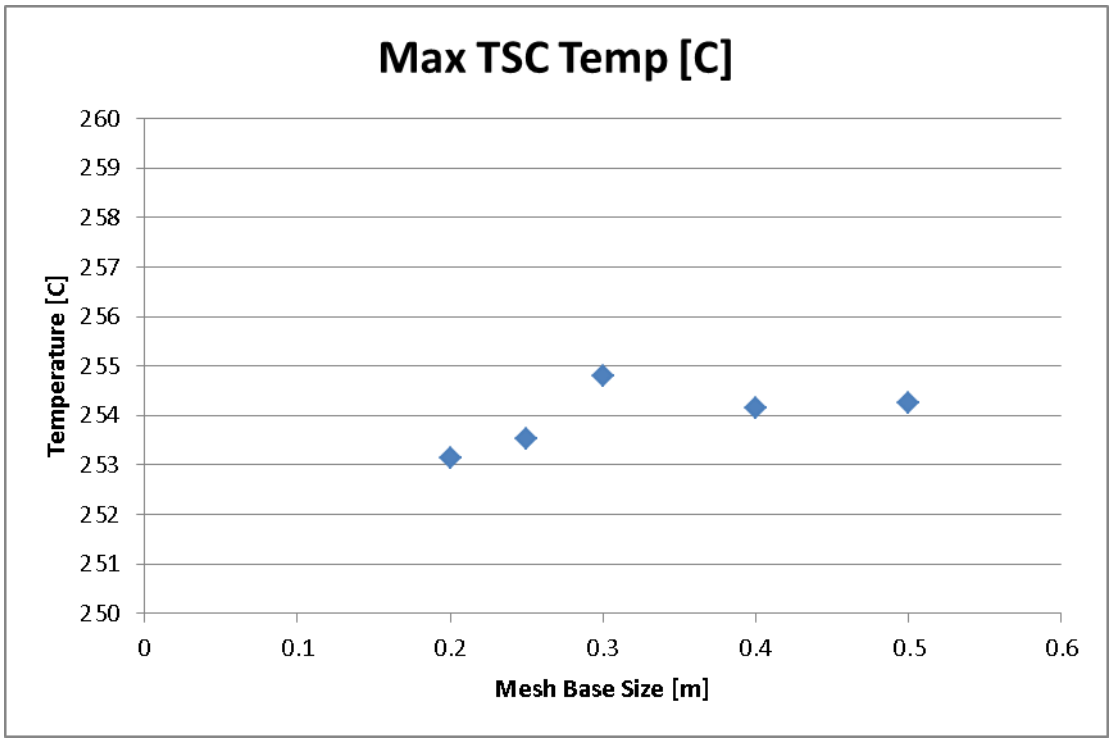

Figure 5-6. Mesh Sensitivity Study – Peak TSC Shell Temperature Results

5.2 Material Properties

Temperature-dependent properties were used in the STAR-CCM+ model for all solids and for both gases (air and helium). For thermal conductivity and dynamic viscosity of air, this was accomplished with appropriate inputs to Sutherland's law, an option available in the code. These same properties for helium were included in the STAR-CCM+ model as user-defined input tables (Incropera et al. 2007).

Since the helium in the TSC does not communicate with an external pressure boundary, the gases were assigned a constant density and buoyancy forces were computed using the Boussinesq approximation (see Cuta et al. 2013, Section 6.1.1). The helium gas density was set to the target bulk gas density of 0.76 kg/m^3 cited in the FSAR. Since the airflow has pressures referenced to inlet and outlet boundaries, air density was computed using the ideal gas law.

The helium within the TSC is modeled as a laminar flow. The cooling airflow was modeled as a turbulent flow using the built-in k-omega SST turbulence model (CD-adapco 2015).

5.3 Approximation of Fuel Region

Following general practice for CFD models of baskets and fuel assemblies, the rod bundles are modeled as a homogenized medium, with average properties designed to simulate heat transfer from the fuel and to give a representative and conservative representation of peak fuel temperatures. This strategy is well tested in horizontal storage systems where heat transfer by thermal conduction and radiation dominate and the contribution from convection in the fuel assemblies is small enough to be negligible. In such conditions, the radial heat transfer in the

fuel is modeled as conduction-only with an effective thermal conductivity that includes effects of thermal radiation, following the methodology in Bahney and Lotz (1996).

The approximate treatment of the fuel region in a vertical storage arrangement is a greater challenge because convective heat transfer can be significant. For this to occur, the basket needs to be open enough to provide a sufficient path for fill gas recirculation. There is plentiful open space within the MAGNASTOR TSC between the outer shell and the basket assembly and there is no significant blockage of return flow to the bottom of the fuel tube array. As such, it is expected that significant natural convection will occur in the TSC, as a function of decay heat loading of the basket. In this case the fuel region is modeled as a porous media with loss coefficients that give a representative mass flow rate of the circulating gas. Losses through assembly nozzles/fittings and across distributor plates can be significant. The validity of the effective thermal conductivity model in this case is not extensively validated against relevant experimental data, but it is widely used in the nuclear industry nonetheless. An example of a porous media model of a TN24 cask is provided in Brewster et al. (2012).

For the present model, the porous media implementation for convection is described first in Section 5.3.1. Section 5.3.2 describes details of a method to impose the desired effective thermal conductivity in the radial direction, within the framework of a typical CFD code.

5.3.1 Porous Flow

Porous media loss coefficients had been previously developed for Westinghouse Electric Company (WE) 17x17 OFA fuel using data from the now defunct OCRWM[9] database (DOE 1992, DOE 1981). These loss coefficients were used to represent the 17x17 fuel in the Catawba TSC. A summary of these coefficients and how they were computed is provided in this section.

A 3D CAD representation of the gas space within the 17x17 fuel assembly was generated and used to create a STAR-CCM+ flow model. The geometry and mesh for the flow model are shown in Figures 5-7 and 5-8. This model was used to determine the axial and radial pressure distribution across the fuel assembly at different input velocities. Figure 5-9 shows the resulting pressure drop versus velocity plot.

[9] DOE Office of Civilian Radioactive Waste Management.

Figure 5-7. CAD Geometry of Gas Region of WE 17x17 OFA

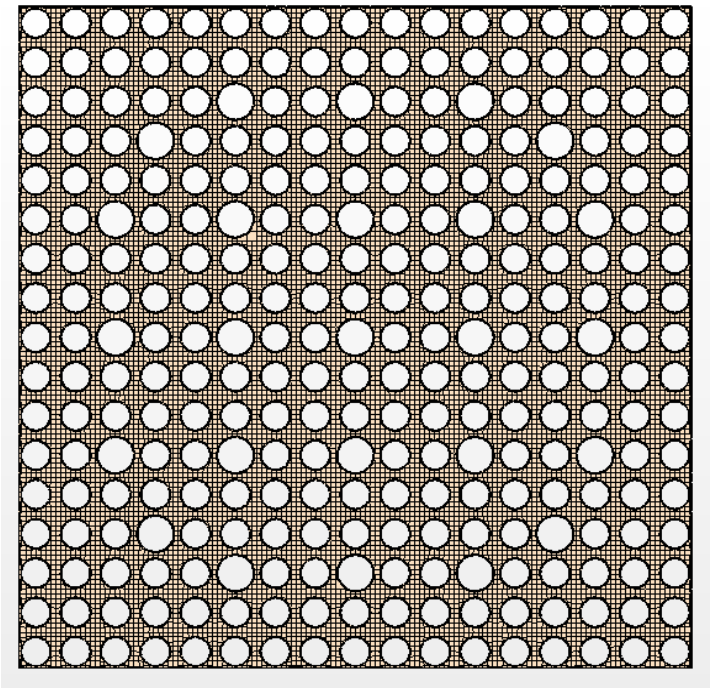

Figure 5-8. Cross-sectional View of Mesh for WE 17x17 OFA

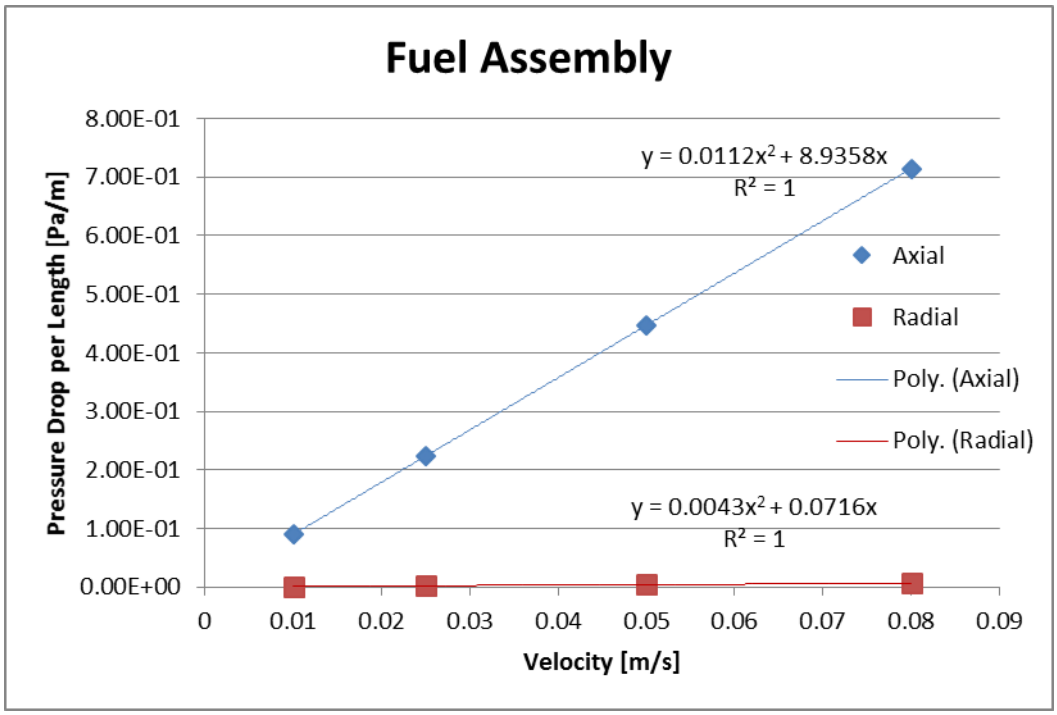

Figure 5-9. Radial and Axial Plots of Pressure Drop versus Velocity for WE 17x17 OFA

The data from Figure 5-9 was used to calculate the inertial and viscous coefficients in both the radial and axial direction using the following equation (CD-adapco 2015):

$$\frac{\Delta P}{L} = -(\alpha v + \beta)v \tag{5.1}$$

where

ΔP = pressure delta
L = length
α = inertial coefficient
β = viscous coefficient
v = normal velocity

The fit equations from the data and trend lines in Figure 5-9 are in the same form as equation 5.1, resulting in the coefficients corresponding to the inertial and viscous coefficients. These coefficients are shown in Table 5-1. The inertial and viscous coefficients are used to calculate pressure losses in each assembly in the porous media model within STAR-CCM+. The volume of the CAD geometry was also used to calculate the void fraction of the fuel assembly. The void fraction is defined as the fraction of porous volume that is occupied by the gas. The volume occupied by the gas was divided by the total volume of the fuel assembly to determine the void fraction. A void fraction of 0.5265 was calculated for WE 17x17 OFA.

Table 5-1. Radial and Axial Porosity Coefficients for WE 17x17 OFA Fuel Assembly

	Fuel Assembly	
	inertial coefficient α [kg/m^4]	viscous coefficient β [kg/m^3-s]
axial	0.0112	8.9358
radial	0.0043	0.0716

A CAD geometry and flow model was also built for a simplified lower fitting of the 17x17 fuel assembly, and the same process was used to determine the porous media model inputs (i.e., void fraction, inertial, and viscous coefficients). Figure 5-10 shows the CAD geometry for the gas volume of the lower fitting (the assembly corner supports are omitted from this model). A void fraction of 0.8594 was calculated. The resulting inertial and viscous coefficients are shown in Table 5-2.

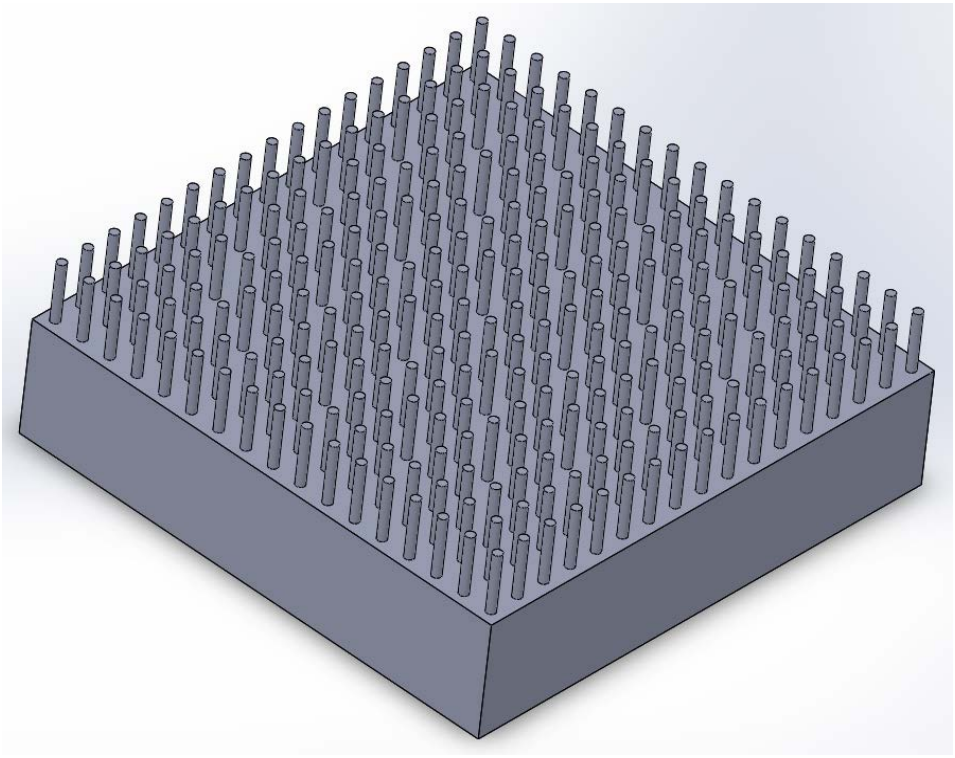

Figure 5-10. Geometry of the Lower Fitting Gas Volume

Table 5-2. Radial and Axial Porosity Coefficients for the Lower Fitting

	Lower Fitting	
	inertial coefficient α [kg/m^4]	viscous coefficient β [kg/m^3-s]
axial	8.5937	4.2475
radial	58.325	3.2774

The upper fitting was assumed to have very little resistance to flow, and to be dominated by a large gas volume. Therefore the upper fitting region was modeled as a helium gas region, and not a porous region.

5.3.2 Effective Thermal Conductivity

The fuel assembly effective conductivity model had also been developed previously and was also based on geometry for WE 17x17 OFA in the OCRWM database (DOE 1987). The effective thermal conductivity model was calculated with an assembly power level of 1.02 kW. Note that the FSAR (NAC 2011) uses 14x14 fuel for design basis thermal analyses, since that fuel configuration has the minimum effective conductivity of all PWR fuel types that can be stored in this system.

The appropriate radial fuel effective conductivity for a given application depends on the fuel assembly geometry, the assembly decay heat, and the geometry of the basket cell in which the fuel assembly resides. The surface emissivity of the fuel rod cladding and the basket cell walls also need to be taken into account in developing an appropriate effective conductivity model for a particular application. For the assumption used in this case, the radial k_{eff} was determined to be,

$$k_{eff_{radial}} = 0.1147\exp(0.0034T) \tag{5.2}$$

where

k_{eff} = effective thermal conductivity (W/m-K)
T = local temperature (K)

For the axial effective conductivity of the assembly, the approach in safety-basis calculations is to neglect thermal radiation in the axial direction and convection. Effective conductivity in the axial direction for the homogeneous block representing the fuel assembly is defined simply as the area-weighted average of the conductivity of zircaloy cladding and helium backfill gas. Conductivity through the fuel pellets is conservatively neglected. A previously developed correlation for this fuel geometry was used in this model.

$$k_{eff_{axial}} = 0.9738\exp(0.0008T) \tag{5.3}$$

The use of these effective thermal conductivities in a porous media representation of the fuel is complicated by the fact that they only apply to the *solid* fraction of the material. The pore space is represented with the properties of the continuous phase, in this case helium.

$$k_{eff_{porous}} = \sigma k_{gas} + (1 - \sigma) k_{solid} \tag{5.4}$$

Since the radial k_{eff} in Eq. (5.2) already represents the combined conduction and radiation heat transfer in the solid rods and surrounding gas, the approach taken here is to apply a correction

$$k_{solid} = (k_{eff_{radial}} - \sigma k_{gas})/(1 - \sigma) \tag{5.5}$$

Since the radial k_{eff} is larger than k_{gas}, this correction increases the solid conductivity by the amount needed to compensate for the porosity-weighted contribution of the lower conductivity of the helium.

This same correction could be used for the axial k_{eff}, however it is less consequential because, in this cask, convection due to recirculation of the helium gas plays a dominant role in axial heat transfer.

5.4 Gap Resistances

The STAR-CCM+ model gap resistances were based on the thermal conductivity and assumed gap thickness between the solid surfaces in the model. An example is shown in the following equation (Incropera et al. 2007):

$$R = \frac{L}{k} \tag{5.6}$$

where

R = contact resistance (m^2-K/W)
L = gap width (m)
k = thermal conductivity of the fluid (W/m-K)

Gap resistances were imposed in same locations as described for the COBRA-SFS model in Section 4.1, except between the assumed layers in the neutron absorber and where a gap was modeled explicitly, as was the case with the gap between the corner basket supports and the inner wall of the TSC. Gap resistances imposed in the STAR-CCM+ model are listed in Table 5-3.

Table 5-3. Gap Resistances Incorporated in the STAR-CCM+ Model

Location	Equivalent Gap Thickness (in.)	Gap Material
Between fuel tubes	0.01	He
Between layers of neutron absorber	0.01	He
Between side support and TSC inner wall	0.1	He
Between support standoffs and TSC outer wall	0.1	Air

5.5 Thermal Radiation

Surface-to-surface thermal radiation within the fuel basket region and thermal radiation from the external surfaces of the cask to the environment are included in the heat transfer evaluations using the STAR-CCM+ model. The surface emissivities used for thermal radiation exchange were set to values shown in Table 5-4. The emissivity used in the STAR-CCM+ model for carbon steel is representative, but differs from the value used in the COBRA-SFS model (see Table 4-1 and footnote on that page).

Table 5-4. Emissivity Values for Radiation Heat Transfer

Material	Emissivity
Carbon Steel	0.65
Concrete	0.8
Stainless Steel	0.46

View factors are computed between patches composed of adjoining cell surfaces. The target ratio of patch count to cell face count was 10%. The thermal radiation model was deactivated in the porous model regions of the fuel assembly because the effective thermal conductivity model in use there already includes radiation.

5.6 External Boundary Conditions

This section describes the various external boundary conditions, including convection on external surfaces, solar loading, and conduction to the ground.

5.6.1 Convection on External Surfaces

Correlations for natural convection between vertical and horizontal surfaces with air at 1 atmosphere were used to calculate the convection heat transfer between the environment and external surfaces. Table 5-5 shows the correlations used (from *Heat Transfer* by J.P. Holman 1996).

Table 5-5. Natural Convection Correlations

Surface	Laminar	Turbulent
	10^4<GrPr<10^9	GrPr>10^9
Vertical plane or cylinder	h=1.42(ΔT/L)^(1/4)	h=1.31(ΔT)^(1/3)
Horizontal plate facing upward	h=1.32(ΔT/L)^(1/4)	h=1.52(ΔT)^(1/3)

5.6.2 Solar Loading

The values used for solar loading are the same regulatory values used in the COBRA-SFS model (as shown in Table 4-2). These are 24-hour average values and they were applied without any reduction for solar absorptivity.

5.6.3 Conduction to Ground

A conduction boundary was applied to the bottom of the storage system model to represent heat transfer to the concrete ISFSI pad. A thermal resistance equivalent to a 3-ft. thick concrete pad was assumed with a 70°F (21.1°C) temperature at its base.

6.0 MODEL RESULTS: COBRA-SFS

This section summarizes the results of thermal evaluations with the COBRA-SFS model of the MAGNASTOR storage system and CNZ-078 canister at Catawba. Section 6.1 presents detailed temperature results for vacuum drying and initial storage (August 2014) and Section 6.2 describes the distribution of temperature by cladding surface area for that same timeframe. Section 6.3 provides temperature results for later storage dates.

6.1 Initial Loading and Storage

The individual assembly total decay heats were illustrated in Section 3.2 for the assemblies loaded into canister CNZ-078, which has a total decay heat estimated as 26.4 kW as of the August 2014 loading date. Section 6.1.1 presents the peak and minimum clad temperatures calculated with the COBRA-SFS model for this initial loading. Section 6.1.2 presents a transient and bounding steady-state evaluation of expected cladding temperatures for vacuum drying conditions. Section 6.1.3 discusses the recirculation within the MAGNASTOR basket.

6.1.1 Initial Storage Conditions

Figure 6-1 and Figure 6-2 show the PCT and the minimum cladding temperatures, respectively, for each assembly, for the as-loaded storage condition.

		266	271	262		
	274	291	294	289	269	
267	292	299	298	296	289	266
273	296	299	301	298	295	273
267	291	298	298	302	292	268
	269	290	295	293	275	
		262	272	267		

Figure 6-1. Assembly PCT (°C) Estimated for Initial Storage Conditions (as of August 2014)

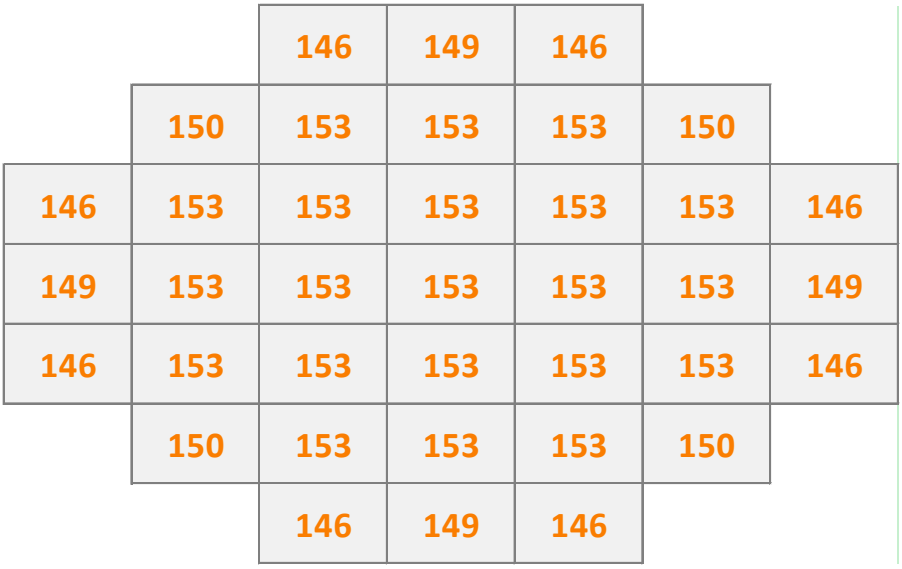

Figure 6-2. Assembly Minimum Cladding Temperatures (°C) Estimated for Initial Storage Conditions (as of August 2014)

These results show when the MAGNASTOR storage system was initially loaded with the CNZ-078 TSC, a reasonable estimate of the maximum PCT is 301°C (573.8°F) on the hottest rod of the center assembly. The minimum clad temperature estimated for this same assembly is 153°C (307.4°F).

The radial distribution of peak component temperatures through the diameter of the cask, including the fuel assembly peak temperatures, is shown in Figure 6-3. The chart in this figure gives the temperature on each component at the axial location of the PCT. Figure 6-4 shows the axial distribution of temperature on the hottest rod in the hottest fuel assembly, along with the axial temperature distribution on the coolest rod in this assembly. The hottest rod is located near the center of the rod array, and the coolest rod is located in the outer corner of the array, reflecting the radial distribution of pin-by-pin decay heat in the assembly, and the simple fact that the walls of the basket enclosing the assembly are the coolest temperatures seen by the rod array for conduction and thermal radiation heat transfer. The same pattern is observed in all assemblies within the basket, with similar variation in the magnitude of the difference between the hottest rod and coolest rod in a given assembly. In general, assemblies at the periphery of the basket have slightly steeper radial temperature gradients than those in the center of the basket.

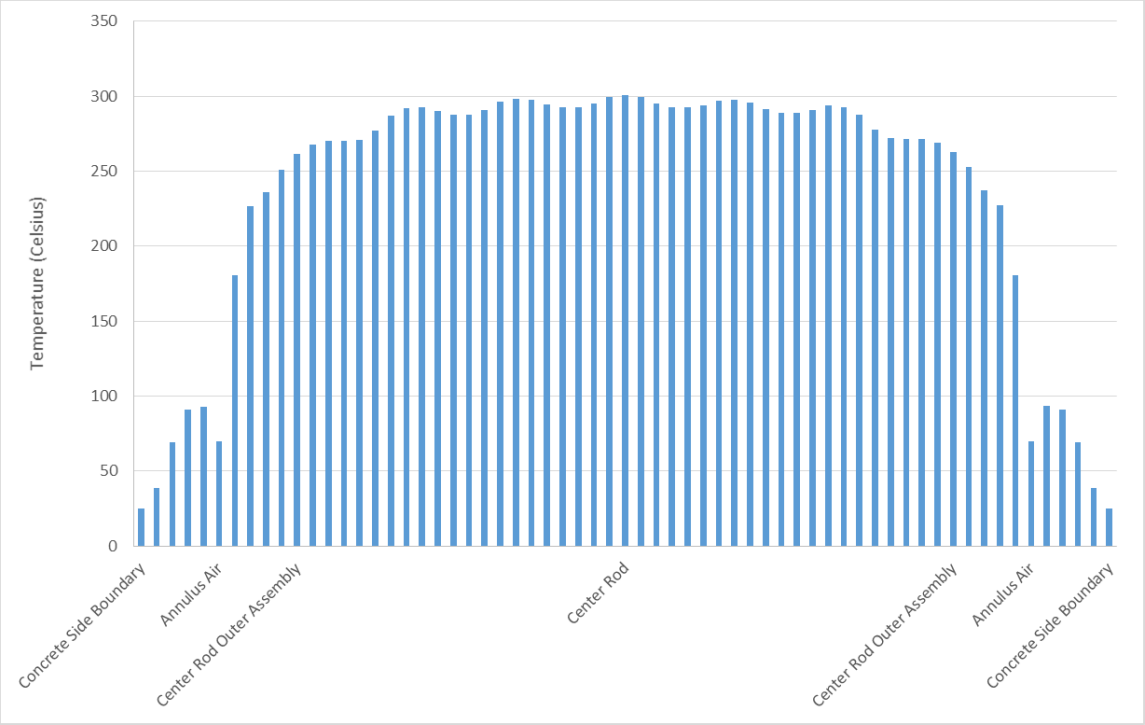

Figure 6-3. Radial Distribution of System Component Temperatures at the Axial Location of PCT for Initial Storage Conditions (as of August 2014)

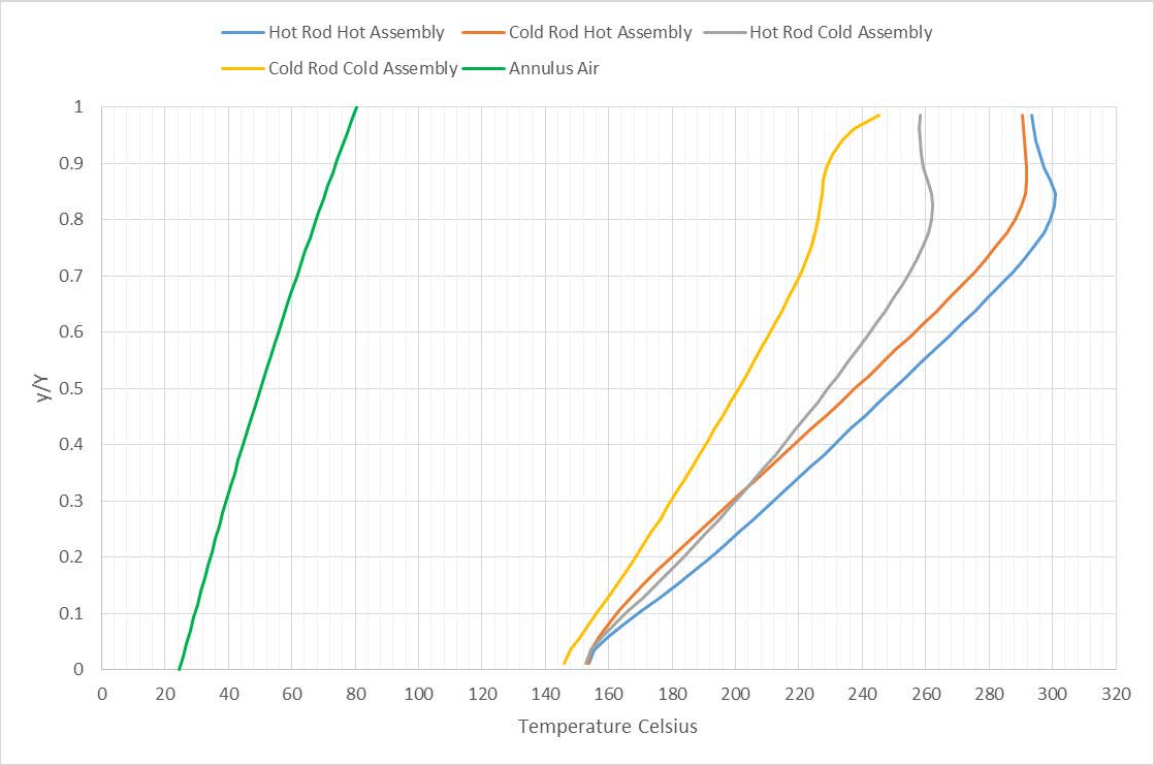

Figure 6-4. Axial Distribution of Temperature of Annulus Air and of Hottest and Coolest Rods in the Hottest and Coldest Assembly for Initial Storage Conditions (August 2014)

6.1.2 Vacuum Drying Conditions

The COBRA-SFS analysis of vacuum drying conditions was performed using the same model (including loading conditions) as described for storage in Section 6.1.1. However the boundary conditions were modified to simulate the conditions seen by the canister during the vacuum drying operations, and the vacuum drying analysis is run as a transient calculation. For this purpose, detailed records were provided by Duke Energy for the vacuum drying procedure for canister CNZ-078. Relevant details from this record are summarized in Table 6-1.

Table 6-1. Timing of Steps in Vacuum Drying and Backfill Operations for CNZ-078

date/time	comments
8/19/2014 (08:21)	start of available data; presumably at or near beginning of transfer operations, with canister and transfer cask annulus full of pool water
8/20/2014 (09:36)	activation of annulus cooling water system (ACWS), circulating water through the annulus between the canister and transfer cask, (inlet temperature nominally 93°F (34°C), very steady for entire duration, where water source is the "spent fuel pool cooling system purification loop"[10])
8/20/2014 (11:09)	estimated beginning of vacuum drying, including interval of siphoning to remove bulk water, at ~1-1.5 atm for several hours, followed by rapid drop to ~5 torr (based on pressure measurements in 2 lines to canister lid)
8/21/2014 (13:42)	estimated end of vacuum drying, based on reported start time of Helium Backfill operation, although pressure measurements continue at low value for an additional 2 hours (to 15:14); data on valving and pump operation incomplete, so some ambiguity in this estimate
8/21/2014 (13:42)	beginning of reported interval of Helium Backfill operation, pressurization line at ~0.1 atm. (basis for minimum estimated vacuum drying interval of 26.8 hours)
8/21/2014 (14:58)	end of reported interval of Helium Backfill operation, instrumentation on pressurization line reporting 6.66 atm. (elapsed time 70.8 minutes (~1.18 hr)
8/21/2014 (15:14)	estimated end of active pumping; end of low pressure measurements (basis for maximum possible vacuum drying interval of 28.08 hours)
8/22/2014 (23:51)	shutting off of cooling water system; water no longer circulating through annulus between canister and transfer cask (no information to indicate when the annulus is drained); total elapsed time of active cooling of canister within transfer cask: 62.25 hours (approx. 2.6 days of continuous operation)
8/23/2014 (02:35)	end of available data; total elapsed time 90.23 hours (approx. 3.8 days)

[10] From comments provided on draft report in September 13, 2016 email from Steve Nesbit (Duke Energy) to Brady Hanson, "MAGNASTOR thermal model report review".

Assumed boundary conditions for the vacuum drying transient include:

1. Constant decay heat of 26.415 kW (initial loading, as per ORNL calculations for fuel exposure and burnup history).
2. Constant temperature of 95°F (35°C) on canister outer shell, including lid and base, as demonstrated by continuous operation of ACWS before, during, and after vacuum drying operation, with measured inlet temperature of 93°F (34°C) and measured outlet temperature of nominally 95°F (35°C) recorded throughout vacuum drying transient.
3. Total vacuum drying time estimated as 28.1 hours.
    a. Includes initial interval of siphoning of bulk water from canister, at nominal pressure of 1 to 1.5 atm, before actual pumping to low pressure begins; estimated from pressure data as approximately 8 hours.
    b. Note that COBRA-SFS transient calculation assumes there is no convection within the canister from the beginning of the vacuum drying interval, and (conservatively) does not capture any effects of heat removed with bulk water removal. This is a typical approach used in normal vacuum drying analyses for SARs and Technical Specifications calculations to define time limits for this step of transfer operations.

The results of the transient calculation are shown in Figure 6-5. At the end of vacuum drying at 28.1 hours the peak cladding temperature is 305.3°C (581.5°F). This is 4°C higher than the peak cladding temperature estimated for storage at initial loading, demonstrating that the peak fuel cladding temperature can be, and in this case is, the highest during drying and transfer operations. In the case of the MAGNASTOR, the TSC is loaded into the storage module (concrete cask) for transport to the ISFSI. However this process takes a significant amount of time during which the annulus water is drained and before which air convection cooling begins after installation in the concrete cask is complete. This final step in the transfer process and its implication to PCT was not investigated, due to lack of information on actual procedures, duration, and boundary conditions for this portion of transfer operations for this TSC.

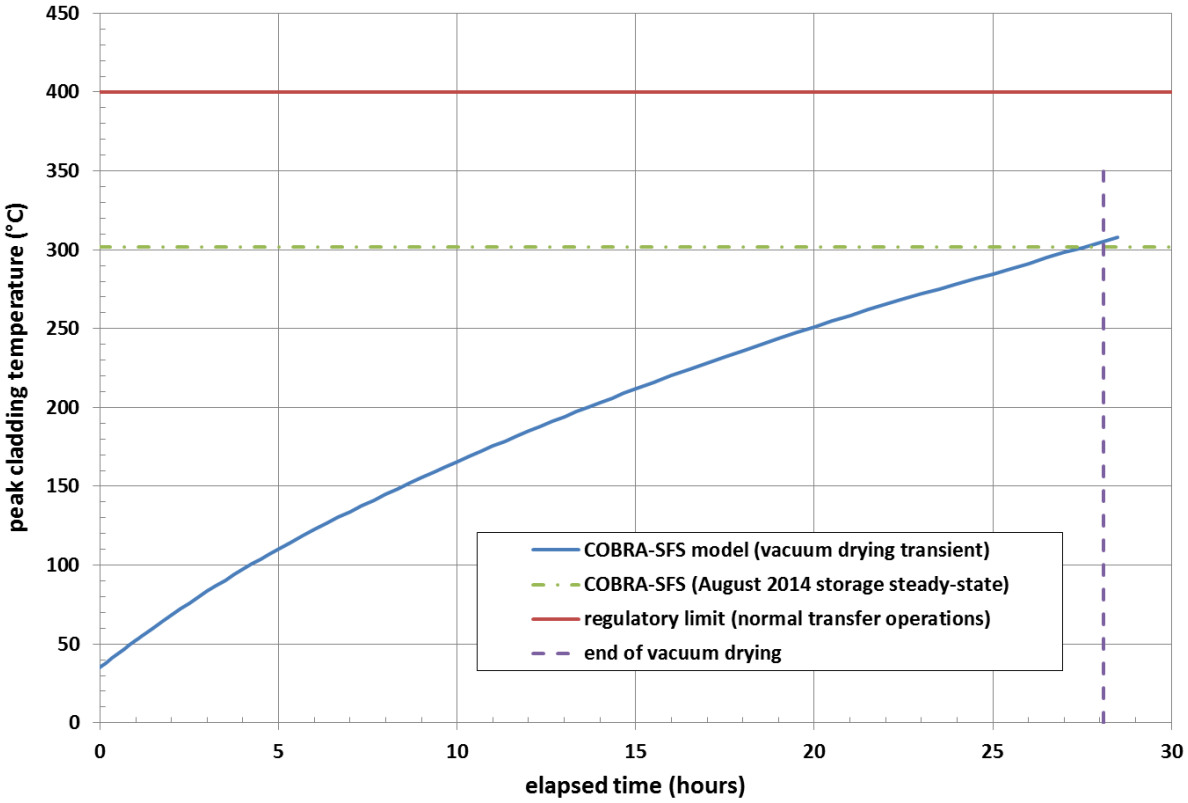

Figure 6-5. Cladding Peak Temperature in Vacuum Drying Transient

6.1.3 Recirculation within the MAGNASTOR Basket

The MAGNASTOR storage system is designed to take advantage of recirculation and the thermo-siphon effect as a primary means of removing heat from the fuel assemblies to the TSC walls. The design features large open flow channels along the length of the basket. For the initial loading case, the COBRA-SFS model predicts helium velocities of up to 0.06 m/s (0.2 ft/s) in the upward direction through the assemblies. The flow then moves downward between the basket and canister wall at as much as 0.12 m/s (0.4 ft/s).

6.2 Summary of Cladding Temperature Distribution

In addition to the PCTs and minimum cladding temperatures reported in Section 6.1.1, the overall distribution of temperature on the fuel rods throughout the demonstration cask is of some interest for evaluations of material performance over time. With 37 assemblies in the cask, each containing nominally 289 fuel pin positions (and up to 264 active rods), the amount of cladding temperature data generated in a single execution of the COBRA-SFS code is considerable. Presentation of this information in a digestible form presents something of a challenge, particularly if the purpose is to convey a three-dimensional picture of the temperature distribution throughout the fuel assemblies in the basket. The axial temperature profiles shown in Section 6.1.1 for the peak rod and the coolest rod of the hottest assembly illustrate the general

shape of the temperature distribution throughout the basket. That is, the highest temperatures occur at about 80% of the height of the fuel assembly, and the lowest temperatures occur near the fuel rod ends. Minimum temperatures are near the bottom of the assemblies, and slightly higher temperatures (but still significantly lower than the peak temperatures) are seen near the upper ends of the fuel rods. The fact that temperatures are not closely aligned with the axial power generation profiles of the rods is due to the high flow recirculation within the basket.

The overall distribution of temperatures throughout the 37 assemblies of the basket has been captured by means of cataloging the temperatures to indicate the fraction of the cladding surface that is expected to be within a given range. Figure 6-6 shows the distribution for all assemblies (as of August 2014), cataloged in increments of 10 degrees-C, from 130°C to 330°C. This interval results in a distribution with about 68% of the cladding surface in the range 200-290°C. Only about 5% of the cladding surface is predicted to be above 290°C, with less than 1% above 300°C. Approximately 28% of the cladding surface is predicted to be below 200°C (392°F) at initial loading.

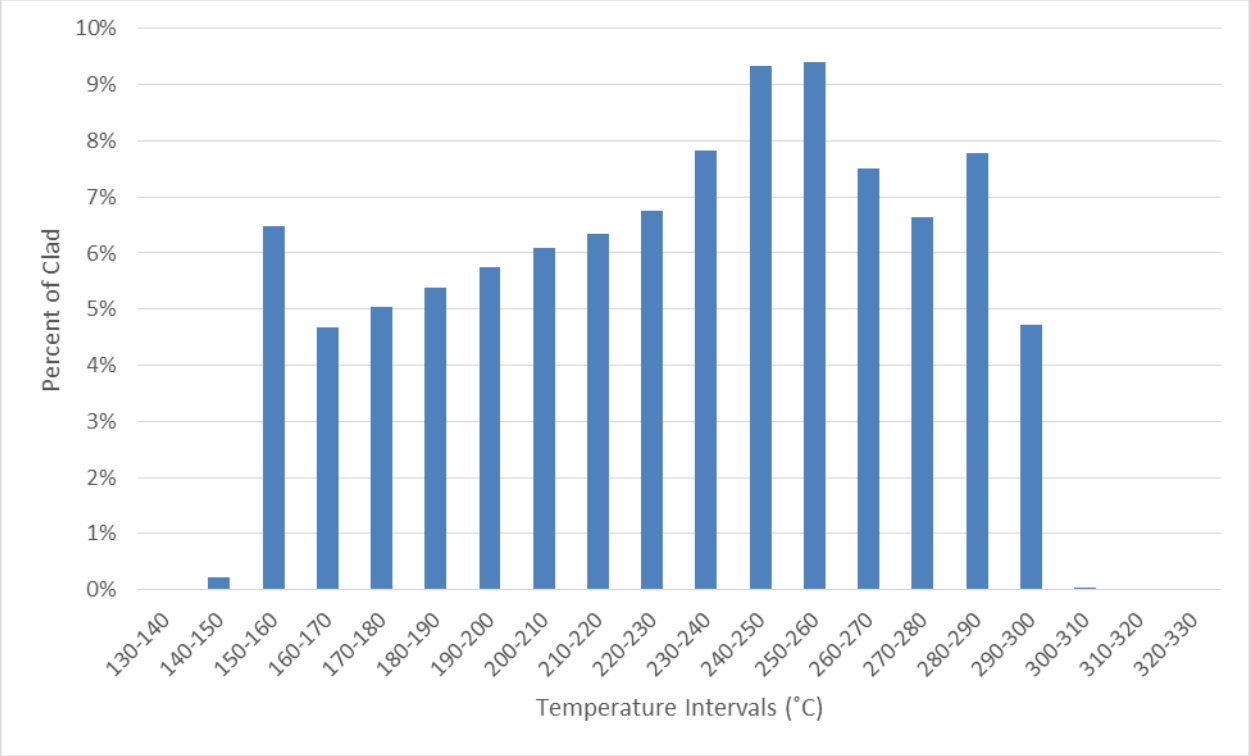

Figure 6-6. Temperature Distribution Ranges for All 37 Assemblies in the Cask, from Cladding Temperatures Predicted with COBRA-SFS Model for Initial Loading Conditions

6.3 Storage Conditions at Future Dates

In this section, analysis results are presented for 10, 50, 100, 200, and 300 years after loading. Figure 6-7 and Figure 6-8 show PCT and minimum cladding temperature, respectively, for each assembly after 10 years of storage. PCT and minimum cladding temperatures for 50, 100, 200, and 300 years of storage are shown in Figures 6-10 through 6-17.

		222	226	219		
	228	241	244	240	224	
224	241	247	246	245	241	224
228	245	246	248	246	245	229
224	240	246	246	246	242	225
	224	240	245	241	229	
		219	227	223		

Figure 6-7. Assembly PCTs (°C) Estimated for End of 10 Years in Storage

		127	129	127		
	130	132	132	132	130	
127	132	133	133	133	132	127
129	132	133	132	133	132	129
127	132	133	133	133	132	127
	130	132	132	132	130	
		127	129	127		

Figure 6-8. Assembly Minimum Cladding Temperatures (°C) Estimated for End of 10 Years in Storage

		145	147	143		
	148	155	157	154	146	
146	155	158	158	157	155	146
149	157	158	158	157	157	149
146	155	157	157	158	156	146
	146	155	157	155	149	
		143	148	146		

Figure 6-9. Assembly Maximum Cladding Temperatures (°C) Estimated for End of 50 Years in Storage

		89	90	89		
	91	92	92	92	91	
89	92	92	92	92	92	89
90	92	92	92	92	92	90
89	92	92	92	92	92	89
	91	92	92	92	91	
		89	90	89		

Figure 6-10. Assembly Minimum Cladding Temperatures (°C) Estimated for End of 50 Years in Storage

		102	104	101		
	104	109	110	108	103	
103	109	111	110	110	109	103
105	110	110	111	110	110	105
103	108	110	110	110	109	103
	103	108	110	108	105	
		101	104	103		

Figure 6-11. Assembly Maximum Cladding Temperatures (°C) Estimated for End of 100 Years in Storage

		66	67	66		
	67	68	68	68	67	
66	68	68	68	68	68	66
67	68	68	68	68	68	67
66	68	68	68	68	68	66
	67	68	68	68	67	
		66	67	66		

Figure 6-12. Assembly Minimum Cladding Temperatures (°C) Estimated for End of 100 Years in Storage

		75	76	74		
	76	79	80	79	75	
75	79	80	80	80	79	75
76	80	80	81	80	80	76
75	79	80	80	80	79	75
	75	79	80	79	76	
		74	76	75		

Figure 6-13. Assembly Maximum Cladding Temperatures (°C) Estimated for End of 200 Years in Storage

		51	52	51		
	52	52	52	52	52	
51	52	52	52	52	52	51
52	52	52	52	52	52	52
51	52	52	52	52	52	51
	52	52	52	52	52	
		51	52	51		

Figure 6-14. Assembly Minimum Cladding Temperatures (°C) Estimated for End of 200 Years in Storage

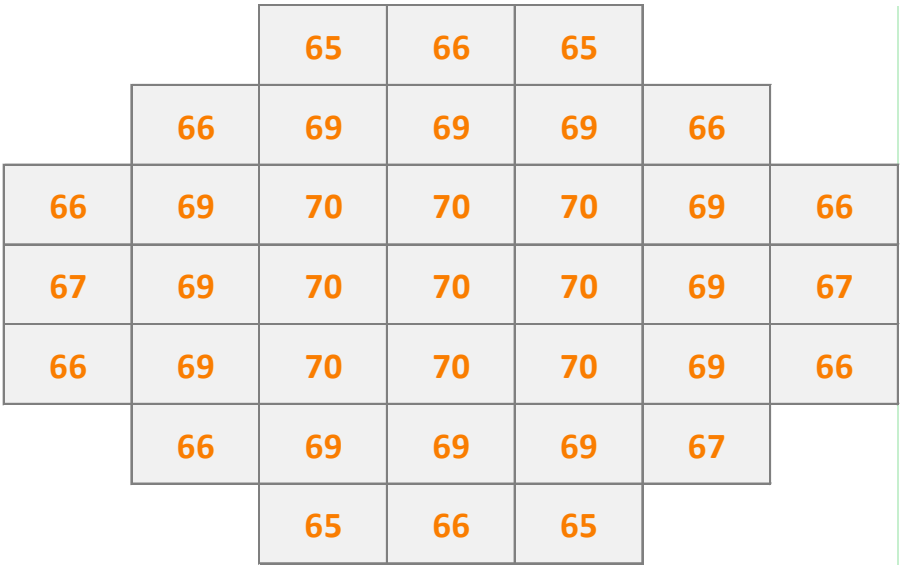

Figure 6-15. Assembly Maximum Cladding Temperatures (°C) Estimated for End of 300 Years in Storage

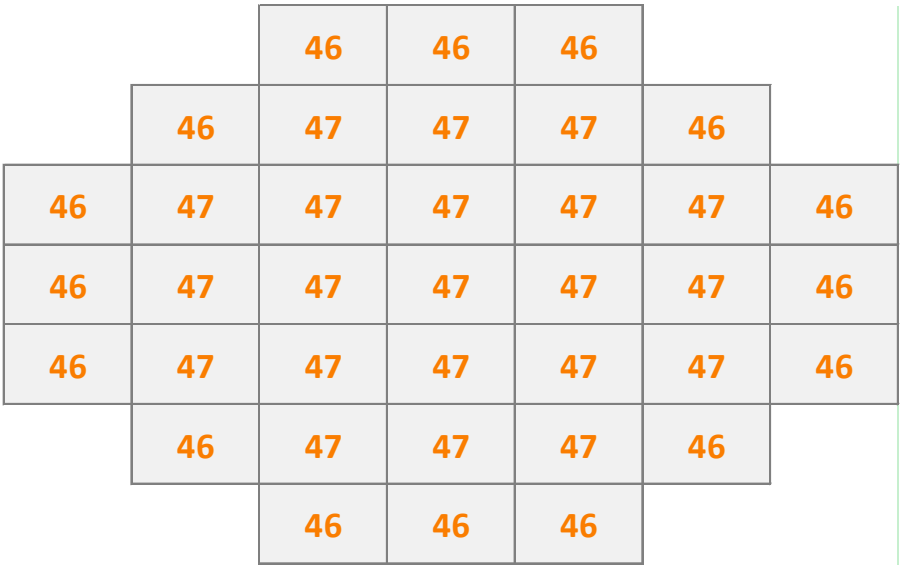

Figure 6-16. Assembly Minimum Cladding Temperatures (°C) Estimated for End of 300 Years in Storage

7.0 MODEL RESULTS: STAR-CCM+

This section of the report presents model results for the decay heat values provided in Section 3.0. Initial model results for design basis loading and for conservative estimates of decay heat are provided in Appendix A.

7.1 Best Estimate Results for Initial Loading in August 2014

The model as described in Section 5.0 was initialized with a uniform temperature equal to the ambient and velocities set to zero. The steady-state solver was run to convergence. The under-relaxation setting for velocity was set to 0.1 and the remaining under-relaxation values were left at their default values. The run was stopped when peak fuel temperature reached a constant value and heat balance between the source decay heat and boundary heat flux was within 0.1%.

The resulting distribution of heat transfer through exterior boundaries is summarized in Table 7-1. As is typical for ventilated storage casks, the bulk of the decay heat is transferred by the cooling air.

Table 7-1. Heat Transfer through Exterior Boundaries

Boundary	Heat Transfer, kW
Cooling air exhaust vents	23.2
Cask circumference	1.8
Cask Lid	1.0
Cask Base	0.3

The distribution of PCTs for each assembly is shown in Figure 7-1.

		261	266	260		
	274	289	292	287	270	
264	290	300	302	297	288	263
269	295	302	307	301	293	269
263	289	300	302	303	290	264
	272	288	293	290	275	
		261	268	264		

Figure 7-1. Assembly PCTs (°C) Estimated with STAR-CCM+ for Initial Loading with Best Estimate Decay Heats

Exterior surface temperatures predicted in this simulation are shown in Figure 7-2.

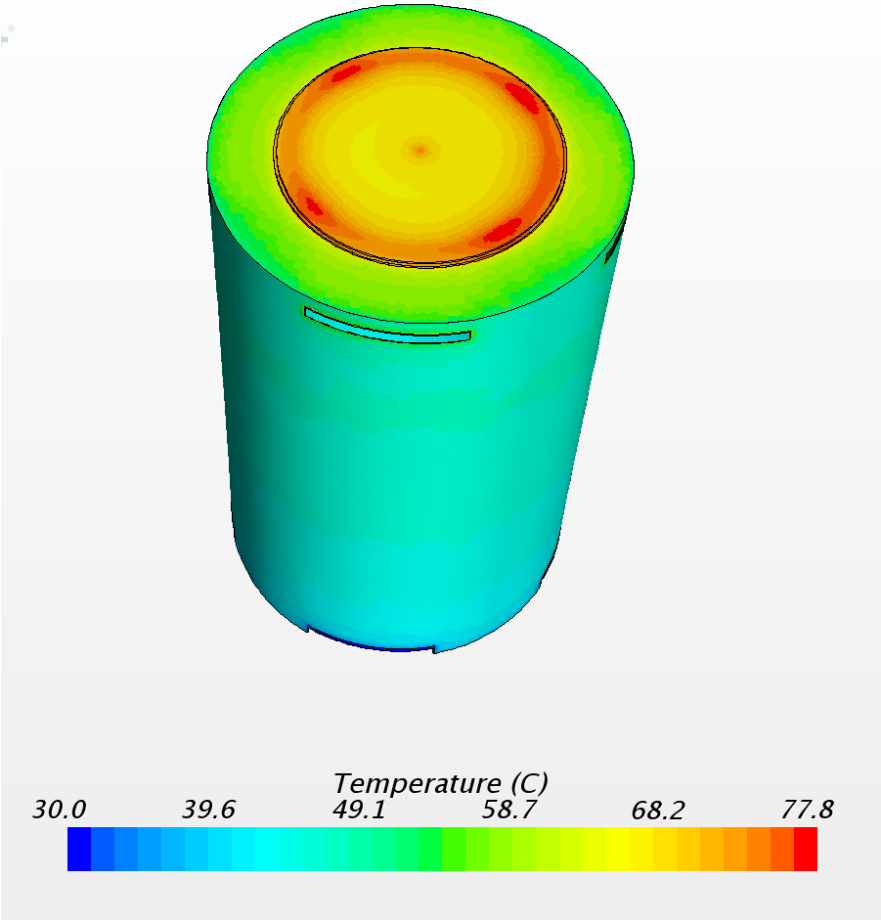

Figure 7-2. Exterior Surface Temperatures

The predicted peak temperature in the fuel region is 307°C (585°F) and this is consistent with the 301°C (574°F) estimate from the COBRA-SFS model (Figure 6-1). The effective thermal conductivity used for the fuel is intentionally conservative, so predicted peak fuel cladding temperatures are expected to be higher than predicted with the detailed fuel model in COBRA-SFS.

The axial distribution of temperatures in the cask is shown in Figure 7-3. The section plane for this plot is through the central row of assemblies.

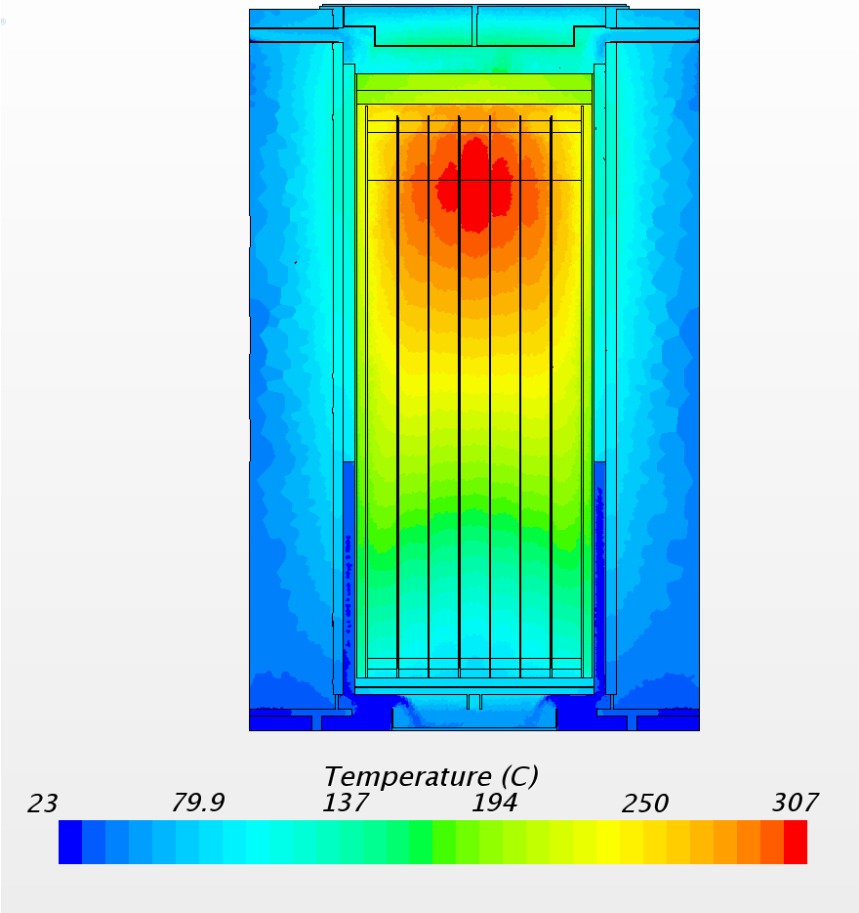

Figure 7-3. Axial Temperature Distribution

Figure 7-4 shows the radial distribution of temperatures at the elevation of the peak fuel temperature. In this view the elevated temperatures within the TSC contrast with the temperature of the cooling air flowing upward in the annulus between the TSC and cask liner. The cask liner and surrounding cask body is hotter than the cooling air because of radiant heat exchange from the TSC and from conduction heat transfer through the standoff spacers.

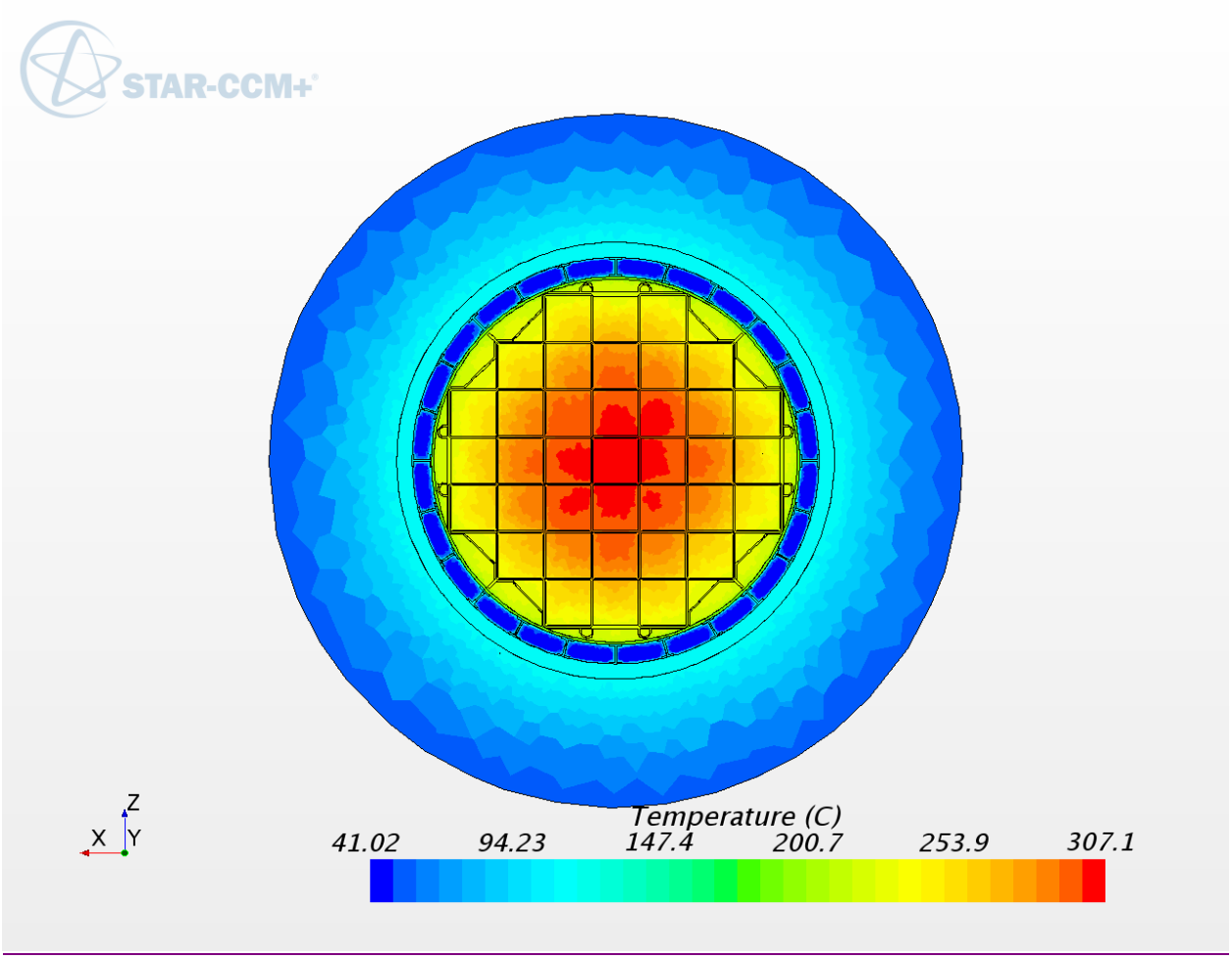

Figure 7-4. Radial Temperature Distribution

The vertical velocity magnitude is shown in Figure 7-5. The view of the cooling airflow in this section is blocked by the standoff spacers, however in the portion of the annulus that is visible, air flow velocities range from approximately 0.7 to 1.0 m/s. The helium velocities inside the TSC are much smaller.

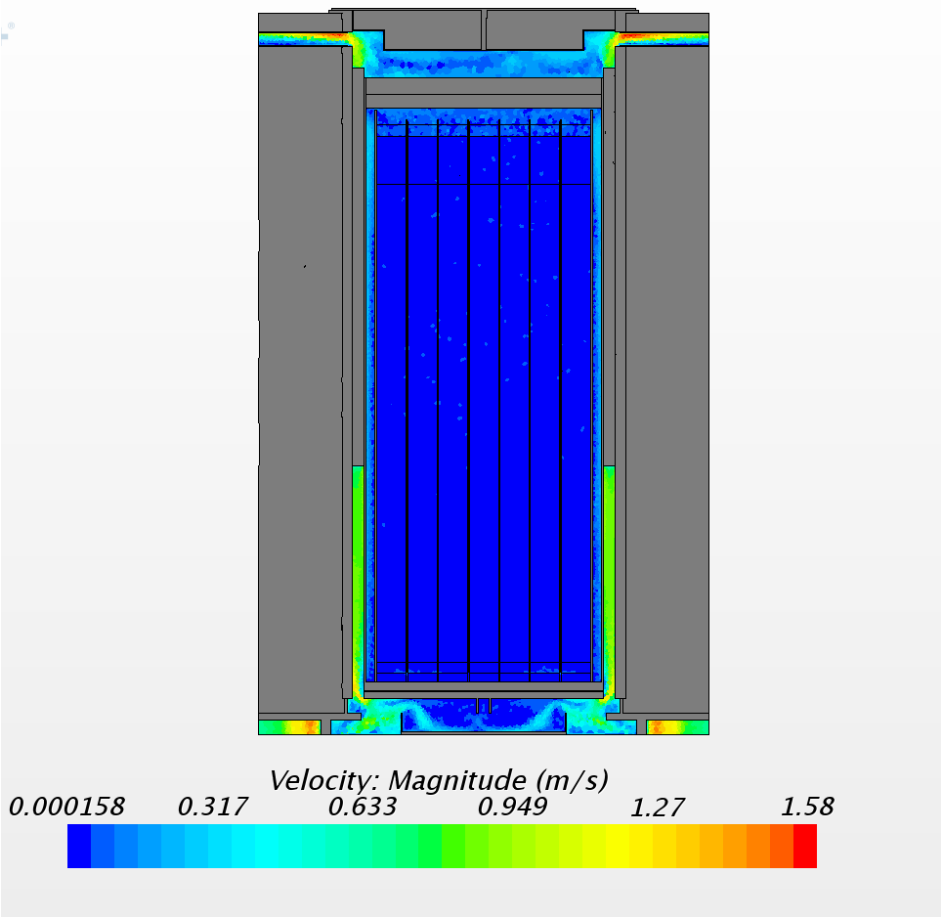

Figure 7-5. Axial Velocity Distribution

The vertical component of the helium velocity in the same section plane are shown in Figure 7-6. Flow upward in the fuel assemblies is only a few cm/s and flow downward in the open sections surrounding the fuel basket range from 0.2 to 0.3 m/s. These velocities are dependent upon the loss coefficients in the porous flow models of the WE 17x17 OFA fuel as described in Section 5.3.1.

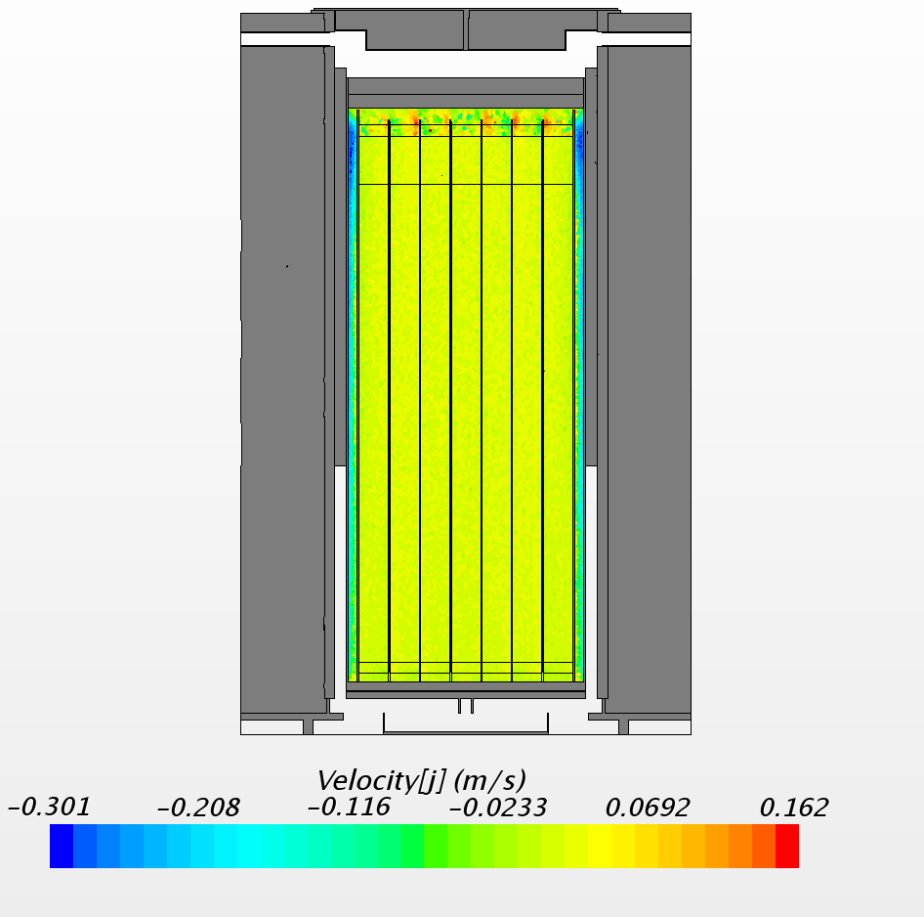

Figure 7-6. Axial Velocity Distribution Inside TSC

The vertical velocity component of cooling air and helium fill gas is shown in the radial section plot in Figure 7-7. The cooling airflow has the highest velocity near the heated walls and standoffs, decreasing to half that velocity in the middle of the flow path. Velocities inside the TSC are all much lower, except for the 0.3 m/s downflow in the outer channels. The helium vertical velocities are shown in more detail at the same section height in Figure 7-8. The upflow velocity in the fuel regions is uniform with a magnitude of roughly 3 cm/s.

The maximum helium velocities in the basket are comparable to maximums computed with the COBRA-SFS model, as reported in Section 6.1.3, when considering that the STAR-CCM+ velocities are averages across the porous media representation of the fuel and the COBRA-SFS maximums are in the flow channels between fuel rods. The peak downflow velocity predicted with STAR-CCM+ in the outer channels is more than twice the value obtained with COBRA-SFS. This is due to the higher mesh resolution in the STAR-CCM+ model and this is consistent with the evidence of higher observed heat transfer from the basket to those channels.

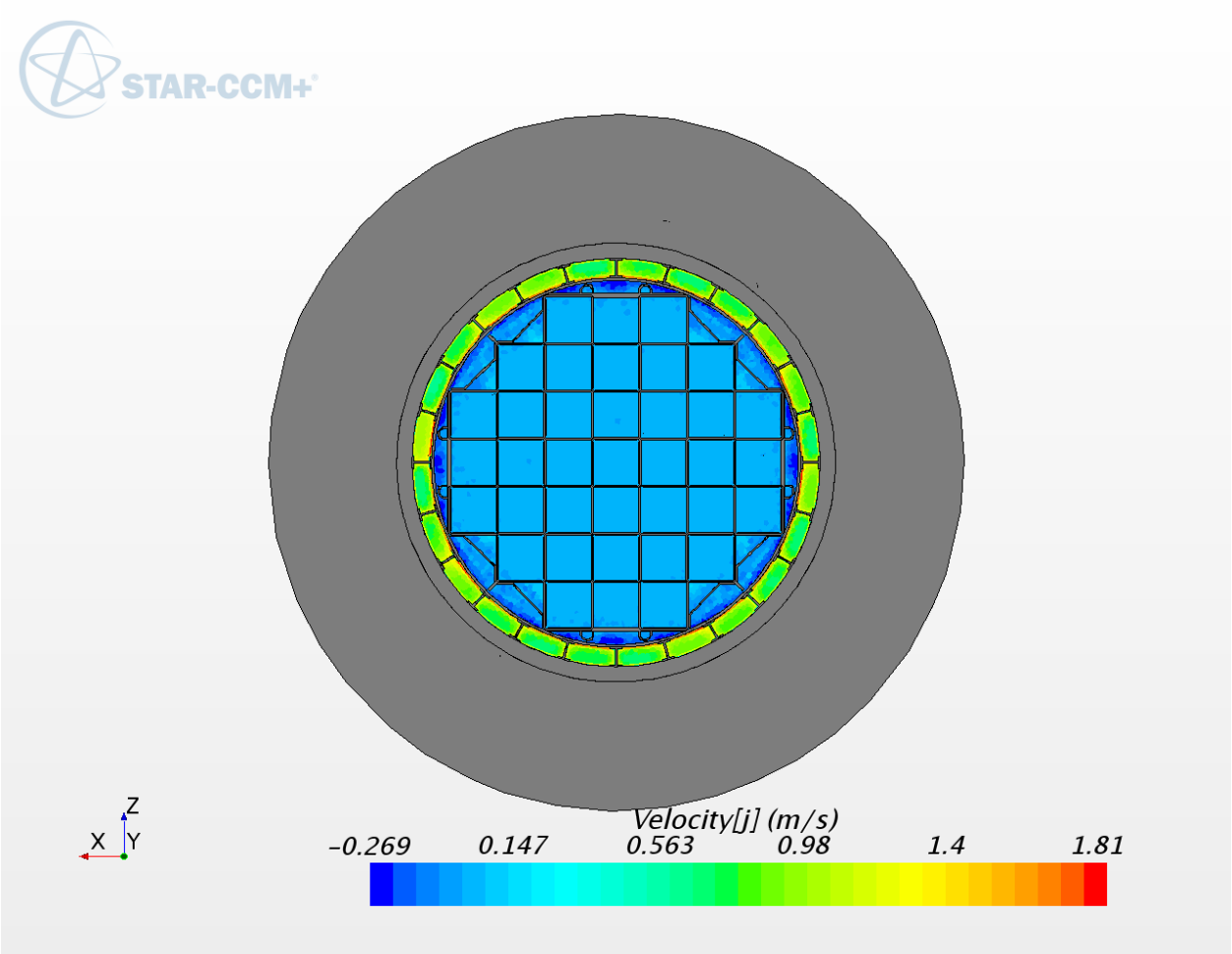

Figure 7-7. Distribution of Vertical Component of Velocity at Mid-Height of Basket

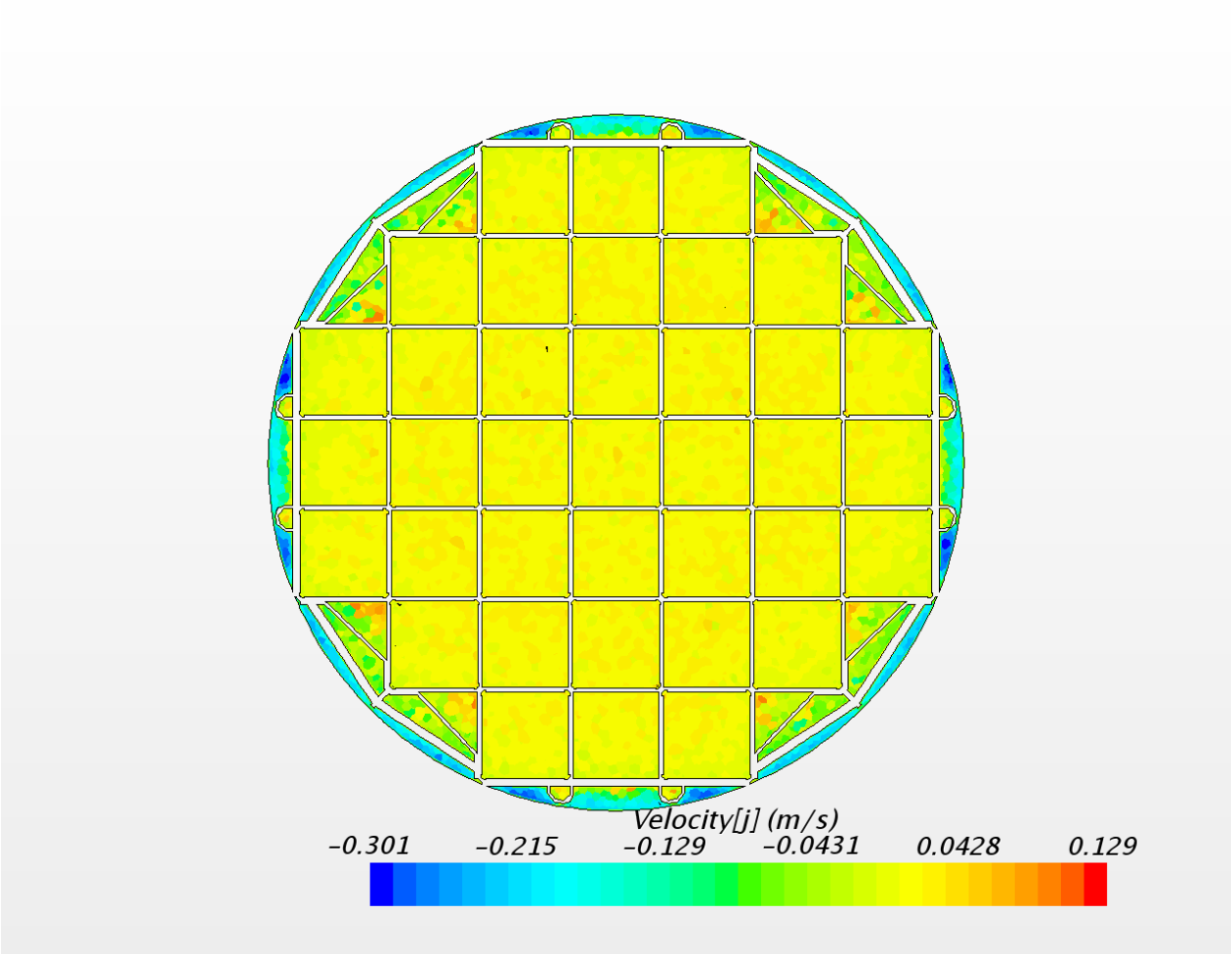

Figure 7-8. Distribution of Vertical Component of Velocity Inside TSC at Mid-Height of Basket

8.0 CONCLUSIONS

Cladding temperatures were estimated for a loaded MAGNASTOR Storage System at Duke Energy's Catawba Nuclear Station. These included estimates at initial loading in August 2014 and projections for storage after 10, 50, 100, 200, and 300 years. The results of this study support the following conclusions:

- Two independent models run with consistent "best-estimate" input values yielded comparable estimates of PCTs in each assembly for the date loaded in August 2014. The peak temperature estimated with the COBRA-SFS model was 301°C and with the STAR-CCM+ model was 307°C.
- Estimates of assembly decay heats calculated using fuel burnup data were 10% lower than the values initially provided by Duke Energy. This is not unexpected as the utility must use conservatively high estimates for the purpose of safety.
- Vacuum drying data provided by Duke Energy showed that the drying operation took 28.1 hours for this cask. A transient calculation performed using COBRA-SFS for this duration and for the boundary temperature in the water-filled annulus showed a reasonable bounding estimate for the peak cladding temperature in vacuum drying would reach 305°C. This estimate is only 4°C higher than the peak predicted for storage conditions with this model.

9.0 REFERENCES

10 CFR 71. 2003. "Packaging and Transportation of Radioactive Material." *Code of Federal Regulations*, U.S. Nuclear Regulatory Commission, Washington D.C.

Bahney III, RH and TL Lotz. 1996. *Spent Nuclear Fuel Effective Thermal Conductivity Report*. BBA000000-01717-5705-00010 Rev. 00, TRW Environmental Safety Systems, Inc., Fairfax, Virginia.

Brewster RA, E Volpenhein, E Baglietto, and CS Bajwa. 2012. "CFD Analyses of the TN-24P PWR Spent Fuel Storage Cask," PVP-2012-78491, in *Proceedings of the ASME 2012 Pressure Vessels and Piping Division Conference*, Toronto, Canada.

CD-adapco. 2015. STAR-CCM+ 10.02 User Guide. CD-adapco, Melville, New York.

Cuta JM, SR Suffield, JA Fort, and HE Adkins. 2013. *Thermal Performance Sensitivity Studies in Support of Material Modeling for Extended Storage of Used Nuclear Fuel*. Fuel Cycle Research and Development, U.S. Department of Energy, Used Fuel Disposition Campaign. FCRD-UFD-2013-000257. PNNL-22646.

Dassault Systemes SolidWorks® Corp. 2011. SolidWorks® Premium 2011 x64 Edition (computer software). Dassault Systemes, Waltham, Massachusetts.

DOE/ET-47912-3. 1981. *Domestic Light Water Fuel Design Evolution*. Vol. 3. Nuclear Assurance Corporation, Atlanta, GA.

DOE/RW-0184. 1987. *Characteristics of Spent Fuel, High-Level Waste, and Other Radioactive Wastes Which May Require Long-term Isolation.* ***Appendix 2A***. *Physical Descriptions of LWR Fuel Assemblies*. Volume 3 of 6. U.S. Department of Energy, Office of Civilian Radioactive Waste Management.

DOE/RW-0184 Rev. 1. 1992. *Characteristics of Potential Repository Wastes*. Volume 1. U.S. Department of Energy, Office of Civilian Radioactive Waste Management.

DOE/RW-0472. 1997. *Topical Report on Actinide-Only Burnup Credit for PWR Spent Nuclear Fuel Packages*. DOE/RW-0472, Revision 1, Office of Civilian Radioactive Waste Management, Washington, D.C.

Fort JA, JM Cuta, SR Suffield and HE Adkins. 2016. *Thermal Modeling of Proposed TN32-B Cask for High Burnup Fuel Storage Demonstration Project*. Fuel Cycle Research and Development, U.S. Department of Energy, Used Fuel Disposition Campaign. FCRD-UFD-2015-000119, PNNL-2549 Revision 1.

Gauld IC, SM Bowman, and JE Horwedel. 2009. *ORIGEN-ARP: Automatic Rapid Processing for Spent Fuel Depletion, Decay, and Source Term Analysis*. ORNL/TM-2005/39, Oak Ridge National Laboratory, Oak Ridge, Tennessee.

Holman JP. 1996. *Heat Transfer*. McGraw-Hill Companies. Edition 8.

Incropera FP, DP Dewitt, TL Bergman, and AS Lavine. 2007. *Fundamentals of Heat and Mass Transfer*. 6th ed. John Wiley & Sons, Hoboken, New Jersey.

Lombardo NJ, JM Cuta, TE Michener, DR Rector, and CL Wheeler. 1986. *COBRA- SFS: A Thermal-Hydraulic Analysis Computer Code; Volume Ill: Validation Assessments*. PNL-6049, Vol. 3, Pacific Northwest Laboratory, Richland, Washington.

Michener TE, DR Rector, JM Cuta, RE Dodge, and CW Enderlin. 1995. *COBRA-SFS: A Thermal-Hydraulic Code for Spent Fuel Storage and Transportation Casks*. PNL-10782, Pacific Northwest National Laboratory, Richland, Washington.

Michener TE, DR Rector, JM Cuta, and HE Adkins, Jr. 2015. *COBRA-SFS: A Thermal-Hydraulic Code for Spent Fuel Storage and Transportation Casks, Cycle 4*. PNNL-24841, Pacific Northwest National Laboratory, Richland, Washington.

NAC 2011. FSAR – Non-Proprietary – MAGNASTOR "Final Safety Analysis Report." Rev. 1, NAC International, Norcrosse, Georgia.

Rearden, B.T. and M.A. Jessee, Eds., *SCALE Code System*, ORNL/TM-2005/39, Version 6.2, Oak Ridge National Laboratory, Oak Ridge, Tennessee (2016). Available from Radiation Safety Information Computational Center as CCC-834.

Rector DR and TE Michener. 1989. *COBRA-SFS Modifications and Cask Model Optimization*. PNL-6706, Pacific Northwest Laboratory, Richland, Washington.

Wieselquist, W.A., A.B. Thompson, J.L. Peterson, and S.M. Bowman. 2016. *ORIGAMI Automator Primer: Automated ORIGEN Source Terms and Spent Fuel Storage Pool Analysis*. ORNL/TM-2015/409. Oak Ridge National Laboratory, Oak Ridge, Tennessee.

Appendix A

Initial Thermal Model Results

Appendix A: Supplemental Thermal Model Results

Model results are provided below for comparison with best estimate values in the body of the report.

A.1 Design Basis Decay Heat Loading

The preferred loading configuration for PWR fuel is shown in Figure A-1. The design decay heat load is 35.5 kW.

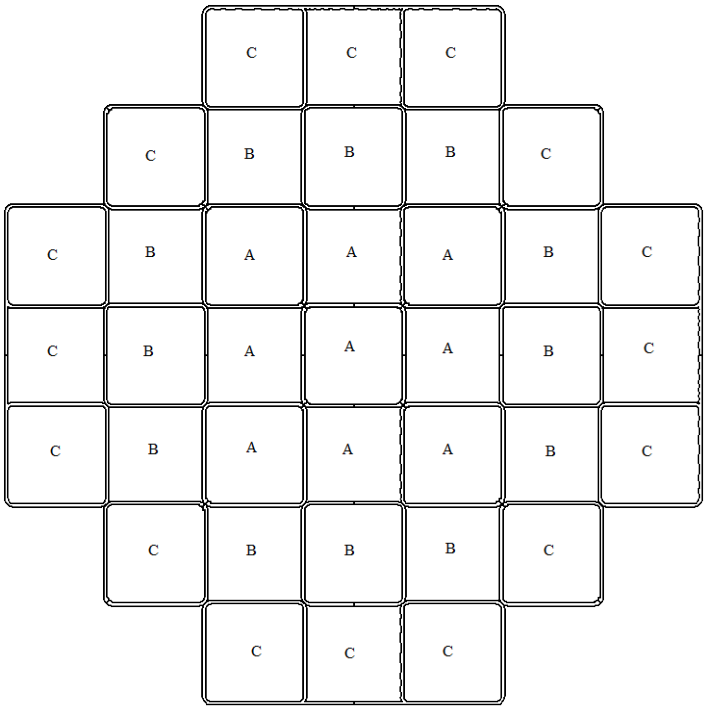

Zone Identification	A	B	C
Maximum Heat Load per Assembly (kW)	0.922	1.20	0.80
Total Number of Fuel Assemblies	9	12	16

Figure A-1. Preferred Loading Map for Design Heat Load (from FSAR, NAC 2011)

The FSAR thermal analysis assumes a simplified axial decay heat profile for PWR fuel. A more realistic distribution was used in the initial models in this Appendix. It is shown in Figure A-2. This axial profile is typical of low-burnup PWR fuel (DOE/RW-0472 1998). Prior studies have shown this profile to also be a reasonable basis for estimating peak clad temperatures in high burnup fuel (Fort et al. 2016).

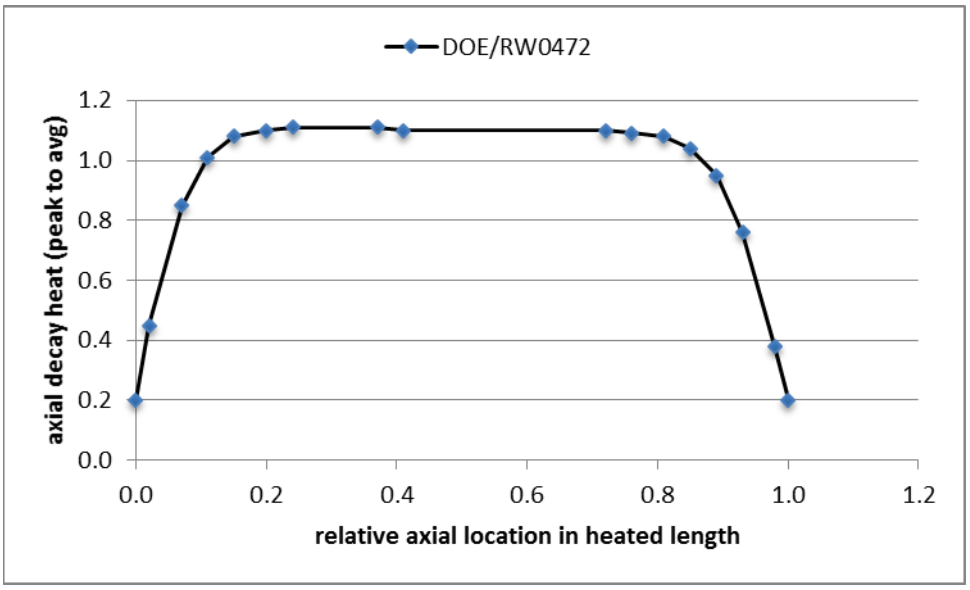

Figure A-2. Bounding Low-Burnup Fuel Profile from DOE/RW-0472 (DOE 1998)

A.1.1 COBRA-SFS Results

		319	324	319		
	328	348	355	348	328	
319	348	354	354	354	348	319
324	355	354	356	354	355	324
319	348	354	354	354	348	319
	328	348	355	348	328	
		319	324	319		

Figure A-3. PCTs (°C) from COBRA-SFS Model for Design Heat Load

		180	182	180		
	183	186	187	186	183	
179	186	187	187	187	186	179
182	187	187	187	187	187	182
179	186	187	187	187	186	179
	183	186	187	186	183	
		179	182	179		

Figure A-4. Minimum Cladding Temperatures (°C) from COBRA-SFS Model for Design Heat Load

A.1.2 STAR-CCM+ Results

The simulation was run with the model as described in Section 4 except for decay heat and axial power profile. The only thermal gap resistance is between basket tubes. No resistance is included between TSC and basket supports and standoff supports. See further discussion and testing regarding these elements in Section A.2 below.

The iterative solution was stopped when the peak fuel temperature reached a steady value and when the balance of heat generation and heat flux through the exterior boundaries agreed within 0.3%. The distribution of heat transfer through exterior boundaries is shown in Table A-1 where the net heat transfer is shown for the cooling airflow.

Table A-1. Heat Transfer through Exterior Boundaries

Boundary	Heat Transfer, kW
Cooling air exhaust vents	31.1
Cask circumference	2.6
Cask Lid	1.4
Cask Base	0.4
Total	**35.5**

The PCTs for each assembly are shown in a cross-sectional representation of the loading map in Figure A-3. The predicted peak temperature in the fuel region is 368°C (694°F) and this is consistent with the 365°C (689°F) estimate in the FSAR (NAC 2011) for similar conditions. This is also consistent with the 356°C (673°F) estimate from COBRA-SFS (Figure A-9-1).

		314	322	315		
	328	348	354	348	328	
315	348	359	362	358	348	315
322	355	363	368	363	354	322
315	347	359	363	359	348	315
	328	347	354	347	328	
		315	322	315		

Figure A-5. PCTs (°C) from STAR-CCM+ Model for Design Heat Load

A.2 As Loaded With Conservative Decay Heat Estimates

The individual assembly decay heats provided by Duke Energy are shown in their relative placement in the TSC in Figure A-7. The total is 29.5 kW, which is 17% below the design value for this storage system. Note that these decay heats are estimates as of the August 2014 loading date.

		753	753	731		
	753	939	936	937	463	
730	969	850	849	849	913	492
731	935	849	848	848	913	731
475	913	848	848	847	913	711
	475	913	913	913	709	
		752	730	730		

Figure A-6. Decay Heat Values from Duke Energy for TSC CNZ078 (Watts)

A.2.1 COBRA-SFS Results

The values of peak and minimum cladding temperatures calculated with COBRA-SFS for the conservative decay heat estimates are shown in Figures A-8 and A-9, respectively. Axial temperature profiles for the hottest assembly are shown in Figure A-10 and a radial distribution of component temperatures is shown in Figure A-11. Finally, a distribution of fuel cladding temperatures is provided in Figure A-12.

		289	296	288		
	297	317	321	315	291	
288	317	325	326	324	313	283
294	321	326	328	325	320	293
283	314	324	326	324	315	288
	291	314	320	315	296	
		288	295	288		

Figure A-7. Estimated Assembly Peak Clad Temperatures for Conservative Loading (°C)

		156	159	156		
	160	163	164	163	160	
156	163	164	164	164	163	156
159	164	164	164	164	164	159
156	163	164	164	164	163	156
	160	163	164	163	160	
		156	159	156		

Figure A-8. Estimated Assembly Peak Clad Temperatures for Conservative Loading (°C)

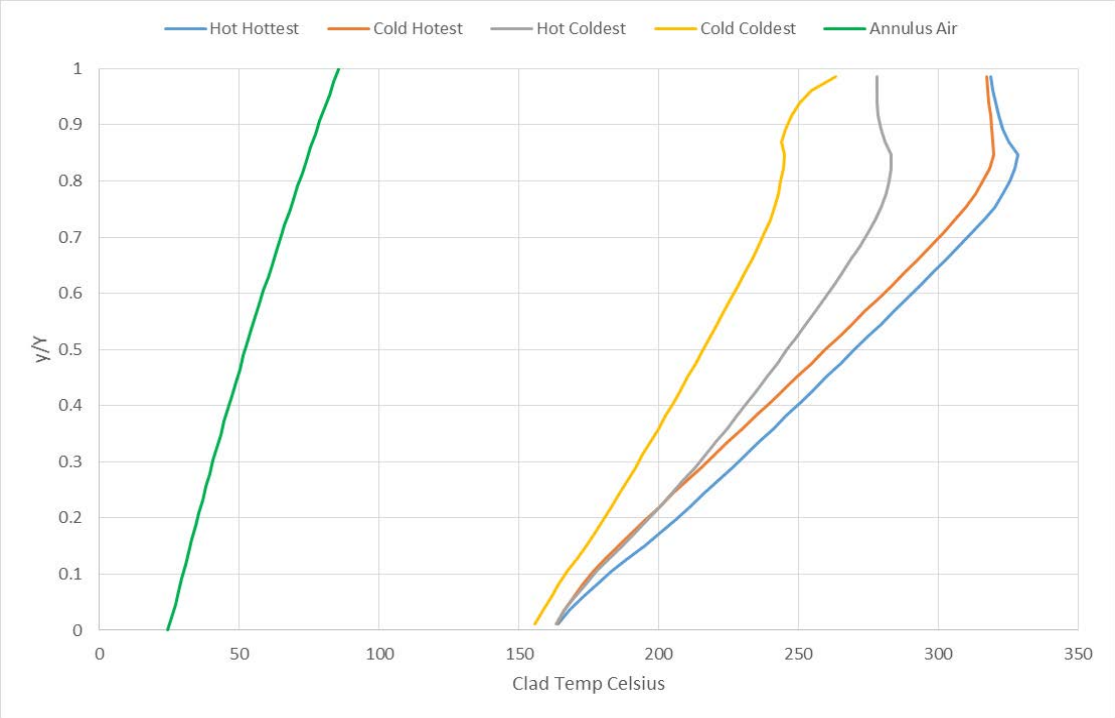

Figure A-9. Axial Distribution of Temperature of Annulus Air and of Hottest and Coolest Rods in the Hottest and Coldest Assembly for Conservative Loading

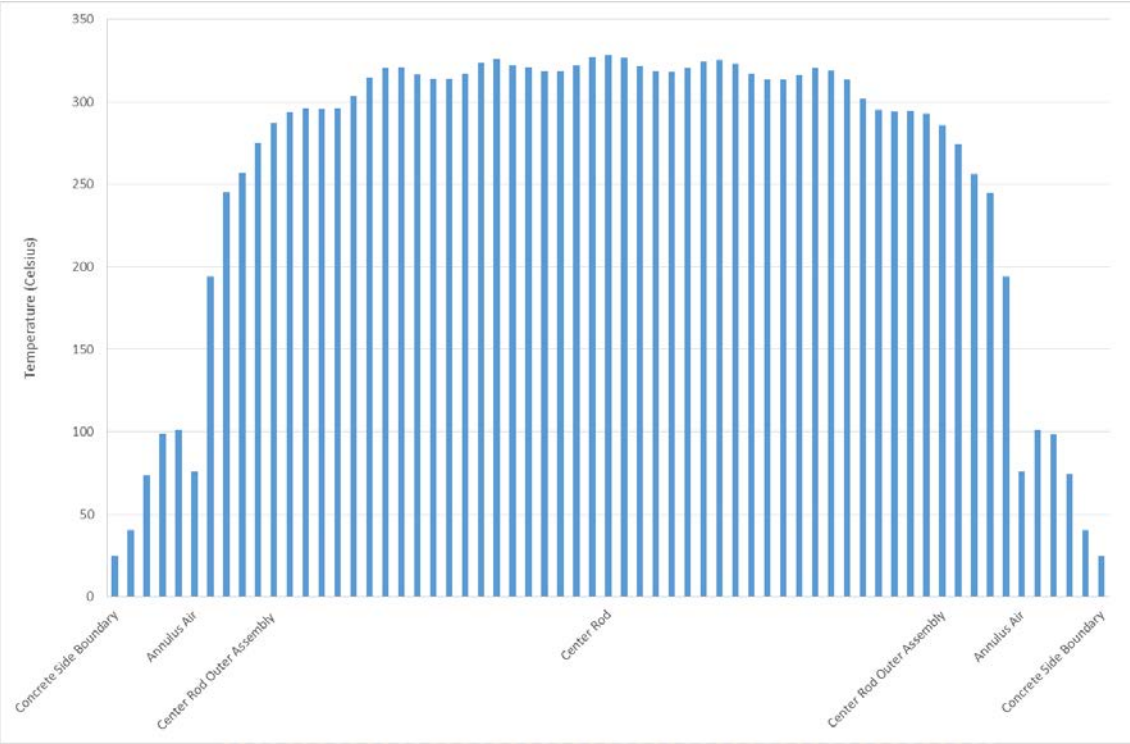

Figure A-10. Radial Distribution of System Component Temperatures at the Axial Location of PCT for Initial Storage Conditions

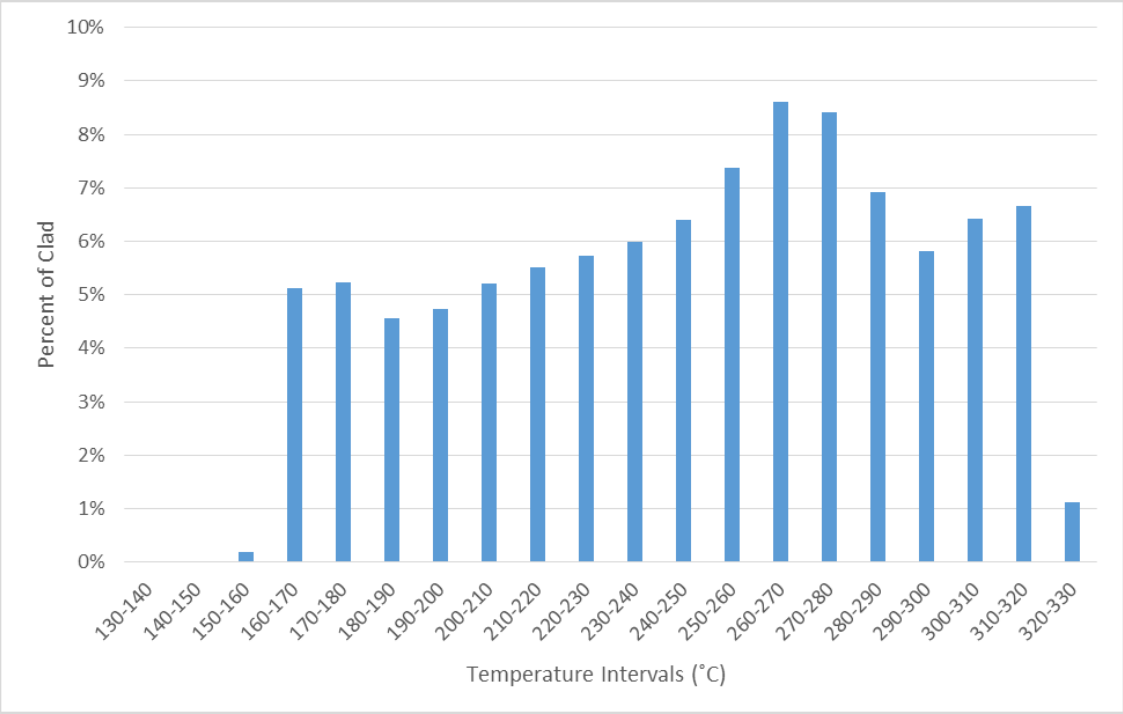

Figure A-11. Temperature Distribution Ranges for All 37 Assemblies in the Cask, from Cladding Temperatures Predicted with COBRA-SFS Model for Conservative Loading

A.2.2 STAR-CCM+ Results

The distribution of heat transfer through exterior boundaries is shown in Table A-2 where the net heat transfer is shown for the cooling airflow.

Table A-2. Heat Transfer through Exterior Boundaries

Boundary	Heat Transfer, kW
Cooling air exhaust vents	25.9
Cask circumference	2.1
Cask Lid	1.1
Cask Base	0.4
Total	**29.5**

The PCTs for each assembly are shown in Figure A-13. These values are consistent with the 328°C (622°F) estimate from COBRA-SFS (Figure A-8).

		283	289	283		
	297	313	317	312	292	
284	312	324	326	323	311	280
288	316	326	332	326	315	287
280	311	323	326	323	311	282
	292	311	316	312	294	
		283	289	283		

Figure A-12. PCTs (°C) from STAR-CCM+ Model for CNZ-078 with Conservative Decay Heat Estimates

A.3 Appendix References

DOE/RW-0472. 1998. *Topical Report on Actinide-Only Burnup Credit for PWR Spent Nuclear Fuel Packages*. DOE/RW-0472, Revision 2, Office of Civilian Radioactive Waste Management, Washington D.C.

NAC 2011. FSAR – Non-Proprietary – MAGNASTOR "Final Safety Analysis Report." Rev. 1, NAC International, Norcrosse, Georgia.